Available online at www.sciencedirect.com
ScienceDirect
Journal of Electroanalytical Chemistry 604 (2007) 72–90
Journal of Electroanalytical Chemistry
www.elsevier.com/locate/jelechem

Analytical approach to polymer electrolyte membrane fuel cell performance and optimization

Prodip K. Das [a], Xianguo Li [a,*], Zhong-Sheng Liu [b]

[a] Department of Mechanical Engineering, University of Waterloo, Waterloo, Ont., Canada N2L3G1
[b] Institute for Fuel Cell Innovation, National Research Council, Vancouver, BC, Canada V6T1W5

Received 21 November 2006; received in revised form 16 February 2007; accepted 21 February 2007
Available online 28 February 2007

Abstract

The performance of polymer electrolyte membrane (PEM) fuel cell is mainly influenced by ohmic, activation, and concentration overpotentials. Ohmic overpotential is directly proportional to electric resistance in the fuel cell components that can be estimated from the experimental data or from the empirical relation for the cell polarization curve. However, such simple relation is not available for the activation overpotential; hence a need exists to develop simple analytical formulation for calculating activation overpotential. In this study, an analytical expression for the activation overpotential in the cathode catalyst layer has been developed to investigate the performance and optimization of a PEM fuel cell. It is found that the analytical expression of activation overpotential with the combination of proper estimates of ohmic overpotential has accurate predictive capabilities. It also provides an excellent agreement with available experimental, numerical, and empirical results. Following this, a performance optimization of cathode catalyst layer in PEM fuel cells has been carried out. It is observed that in a typical PEM fuel cell, excess platinum is neither desirable nor favorable. The optimum platinum loading is found to be 0.19–0.20 mg/cm^2 when the cell output is set to 0.8 V. The higher the membrane content in the catalyst layer, the better the cell performance in terms of activation overpotential. Conversely, optimum catalyst layer thickness is found to be 9–11 μm for the platinum loading of 0.20 mg/cm^2 at the cell voltage of 0.8 V. It is found desirable for the catalyst layer slightly thicker than the optimum value as the cell performance is less sensitive then; whereas performance decreases rapidly if the thickness of the catalyst layer is below the optimum value.

Keywords: Polymer electrolyte membrane (PEM) fuel cells; Cathode catalyst layer; Activation overpotential; Optimization

1. Introduction

Polymer electrolyte membrane (PEM) fuel cell was first used in the 1960s in NASAs Gemini space flights as an auxiliary power source. However, it was dormant for almost over 20 years since its first application. Recently, a "quantum jumps" has been observed in the PEM fuel cell research as it can be one of the most promising candidates for the next generation power sources [1,2]. In addition, its high power density; low operating temperature; quick start-up; fast dynamic response; and most importantly zero emission capabilities open up opportunities to wide practical use in portable, mobile, and stationary cogeneration applications [3]. Particularly, its zero emission capabilities can reduce greenhouse gases as well as will mitigate concerns about the global warming and global climate change. Although the scientific principle behind the PEM fuel cell technology is well established, success in commercialization depends on optimization of its performance, design, and materials and manufacturing cost. Hence, the development of theoretical model as well as numerical model are required to gain better understanding of the effect of the operating conditions and cell design on the PEM fuel cell performance.

* Corresponding author. Tel.: +1 519 888 4567x36843.
E-mail address: x6li@uwaterloo.ca (X. Li).

0022-0728/$ - see front matter © 2007 Elsevier B.V. All rights reserved.
doi:10.1016/j.jelechem.2007.02.028

Several key processes occur within the PEM fuel cells that have the major impact on the PEM fuel cell performance. The most important processes include the electrochemical reactions in the catalyst layers, proton migration in the polymer electrolyte membrane, and mass transport within all regions of the PEM fuel cell. All these processes have already been addressed in several studies. For instance, Bernardi and Verbrugge [4] provided the mathematical model for oxygen electrode. Later both the hydrogen oxidation and the oxygen reduction reaction in the catalyst layers were modeled assuming fully saturated membrane and water is transported through the electrodes in liquid phase [5]. Siegel et al. [6] developed catalyst layer model considering the catalyst layer void regions to be composed of gas and polymer electrolyte membrane. However, the catalyst layer void regions can be a combination of gas, liquid and polymer electrolyte in the catalyst layers [7]. Conversely, proton migration process in the polymer electrolyte membrane layer has been addressed by Verbrugge and Hill [8] along with water migration in the pores of a fully humidified polymer electrolyte membrane. Since, the protonic conductivity changes with the membrane hydration, Springer et al. [9] developed a PEM fuel cell model in which the protonic conductivity was a function of membrane hydration. In addition to the proton migration model, the water transport processes in the polymer electrolyte membrane layer was modeled by several authors [10–15]. These water-transport models require to solve standard momentum, energy transport, continuity and species concentration equations along with the reaction kinetics in the catalyst layers. Hence all these models are computationally expensive. A completely different water transport model has been proposed by Karimi and Li [16] considering electrokinetic effect. These models later extended into three dimensions to study the complex gas flow and for better gas flow channel designs [17]. Results of these models suggest that in order to be applicable for both saturated and non-saturated gas conditions, water transport model should include two-phase transport, transport in a partially dry membrane and in a fully flooded membrane. Hence, more complex two-phase models have also been developed [18–21]. It is clear from the aforementioned literature review that the evolution of the fuel cell modeling is becoming more and more complex with the advancement of computing power. None of them actually provides any simpler formulation or simple model. Even none of them specifically focused on the individual cell polarization. Whereas polarization occurs in the operation of PEM fuel cells that influences both the performance and the commercialization of the fuel cell.

In addition to the polarization, the other primary factors currently impeding commercialization of PEM fuel cell is the high materials and manufacturing cost. Commonly used Nafion® and platinum (Pt) based electrocatalysts are expensive. Substantial efforts are currently ongoing to reduce the overall fuel cell cost by maximizing the individual cell performance while simultaneously minimizing the amount of electrocatalyst and membrane material used per unit active area. Unless there is a tool for optimizing the amount of expensive materials used during the design of fuel cell as well as the cell polarization, it is impossible to minimize the cost of manufacturing or optimize the performance of the cell. As shown in Fig. 1, among the various losses, the highest irreversible losses in the cell potential occur in the cathode catalyst layer known as activation overpotential, and then followed by the ohmic overpotential. While the losses in the anode catalyst layer are negligible compared to these two losses [22]. Furthermore, there has been mixed potential at the electrodes, which is inherent in PEM fuel cells. It arises due to the unavoidable parasitic reactions that tend to lower the equilibrium electrode potential as well as due to the fuel crossover through the electrolyte membrane. Sometime literature misled and both the mixed electrode potential and the cathode activation overpotential are shown together as activation overpotential [23], which cannot be possible as there always be mixed potential existing in fuel cell operation [24]. To improve the performance, and to design the cost-effective fuel cell, one therefore needs to optimize both cathodic activation overpotential along with the utilization of Pt-catalyst content and membrane content in the catalyst layer. Several studies have already been conducted considering these factors. For instance, an engineering model is used by Marr and Li [25] for performance study of the PEM fuel cell. They provided detailed mathematical formulation for the ohmic overpotential, which can be used in future studies if the cell dimension and material properties are known. This formulation is later used by Baschuk and Li [7] in their parametric study with variable degrees of water flooding in the cathode electrode. Although they incorporated the water flooding parameter, it is not possible to estimate the amount of flooding from this model. The amount of water flooding has been extrapolated by matching the model results with the experimental data of Kim et al. [26]. In addition, both

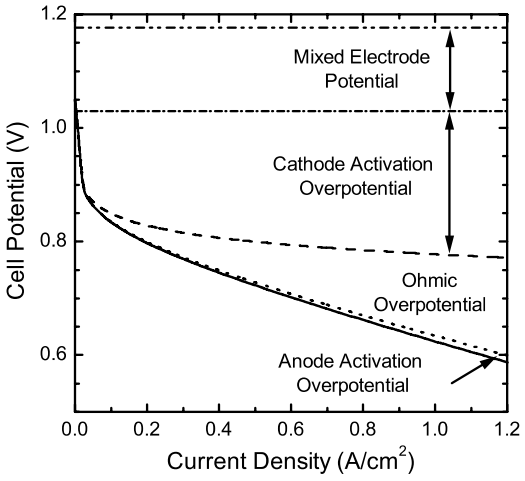

Fig. 1. A typical breakdown of polarization for PEM fuel cells, showing contribution of cathode activation overpotential, anode activation overpotential, ohmic overpotential, and mixed electrode potential.

of these models require numerical solution of several differential equations to estimate the cathode activation overpotential. Rowe and Li [27] produced a one-dimensional, non-isothermal model of a PEM fuel cell to investigate the effect of operating conditions on the cell performance. They also studied the thermal response and the water management to understand the underlying mechanism.

Amphlett et al. [28,29] provided the performance modeling of PEM fuel cell by using a mechanistic approach. They approximated the activation overpotential by Tafel equation and the ohmic overpotential is estimated via Nernst–Plank equation for proton transport through the membrane electrolyte region. They also provided an empirical relation for the internal ohmic resistance from the experimental results of a Ballard Mark IV® fuel cell as a function of cell temperature and current. This empirical relation of the internal ohmic resistance is useful and one can avoid complicated numerical computation during the evaluation of ohmic overpotential. However, this relation is insufficient to capture the change in internal resistance in changing membrane content and fraction of water in the cathode catalyst layer. Similarly, Kim et al. [26] developed an empirical equation using curve-fitting scheme based on experimental data that fits the entire polarization curve of a PEM fuel cell. The inclusion of an exponential term for the mass-transport overpotential (also referred to as concentration overpotential) with an adjustable parametric coefficient was found to accurately model the performance curves up to and including the mass transport limited region at high current densities. Squadrito et al. [30] also provided an empirical expression between the cell potential and the current density similar to Kim et al. [26]. The basic difference in their model is the mass-transport overpotential, which is fitted as logarithmic function instead of exponential function. However, they did not clearly explain the advantage of their model over the model developed by Kim et al. [26]. Once again, their findings are also cell specific. These empirical correlations are dependent on the operating conditions and cell parameters, therefore careful attention is required in using these values in the parametric studies. Nevertheless, the analytical formulation of Marr and Li [22] or the empirical relation of Amphlett et al. [28,29] can provide an approximate estimates of ohmic overpotential, analytical formulation for the cathodic overpotential is still elusive.

The theoretical framework for the analytical solution of the activation overpotential in the cathode catalyst layer has been available either for very low current densities or for large current densities [28,31,32]. Even cathode catalyst layer models are available for small current, fast oxygen diffusion, or fast proton transport [31,33]. None of these previous studies provided the exact analytical solution for the entire range of current densities of the PEM fuel cells. On the optimization side, numerical optimization might be cheap and faster compared to the experimental optimization. Numerical optimization always requires high level of accuracy in the numerical computation as well as a full set of governing equations with well defined boundary conditions. Also formulation of a catalyst layer model is not as simple as ohmic overpotential model. Either macro-homogenous model [4,22], or agglomerate model [34,35] has often been used. Though these models are two extreme cases of catalyst composition, in reality catalyst layer could be in between macro-homogenous and agglomerate models.

The formulation of ohmic overpotential is well established and does not require complicated mathematical formulation or numerical computation for fully hydrated membranes [7,25]. It is mostly dependent on the ohmic resistance of the cell material with the exception of the membrane's resistance, where the amount of water content might change the effective ohmic resistance in some instance. Nevertheless, using these ohmic overpotential formulations, one can optimize the ohmic overpotential; a part of the total polarization of PEM fuel cell except the activation overpotential. Hence, a need exists to develop simple analytical formulation for the cathodic activation overpotential. Here a parametric model for the PEM fuel cell has been developed using a combination of analytical solution and empirical formula, which includes (i) an analytical expression for the activation overpotential in the cathode catalyst layer and its comparison with the various data available in the literature that covers empirical results, experimental data, and numerical predictions. (ii) The composition and performance optimization modeling of the catalyst layer of PEM fuel cell, where Pt-loading, catalyst layer composition, and thickness have been optimized using the analytical model developed in this paper. In the first part, a simple and efficient analytical solution for estimating cathode activation overpotential in the PEM fuel cells is provided that can be used as a bench mark solution to validate future numerical models. In the second part, all design parameters have incorporated in the model for focusing on the cathode catalyst layer optimization including Nafion® content, Pt-content, void fraction, and catalyst layer thickness. The importance of this model is that it can be used to model the performance of fuel cell system as well as it will be a useful tool for optimizing the structures of the membrane electrode assembly, catalyst layer parameters, and cell operating parameters. Investigation has also been conducted for the optimum conditions for Nafion® content, Pt-loading as well as effect of the operating conditions on the performance of PEM fuel cells.

2. Model formulation

In the present study, a typical PEM fuel cell is considered that consists of a cathode and an anode electrode with a proton-conducting membrane as the electrolyte sandwiched in between as shown in Fig. 2a. Generally, the thickness of the electrodes and membrane are approximately 200 μm or smaller [27]. Each of these electrodes also consists of approximately 10 μm (or thinner) catalyst layer between the electrode and the membrane, known as anode

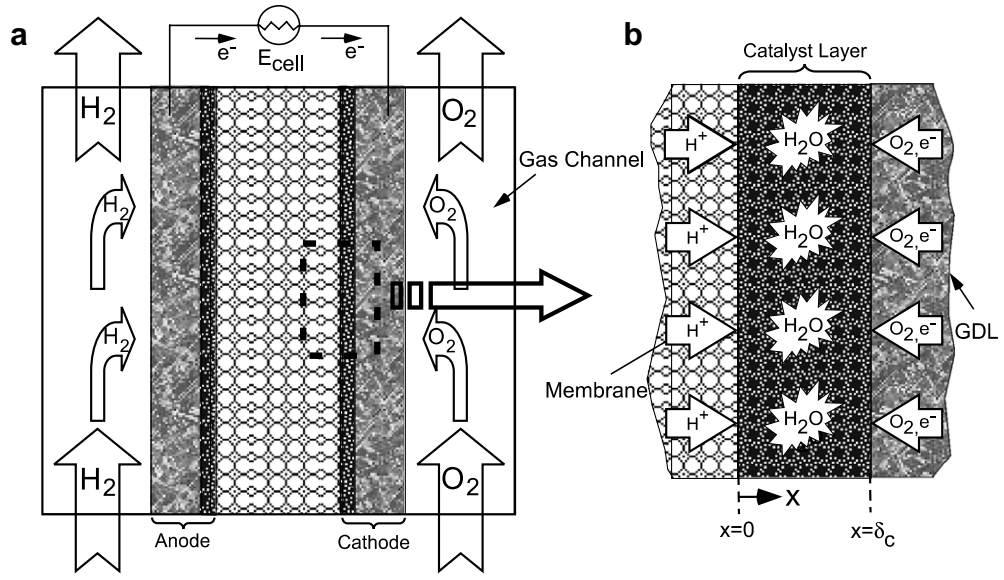

Fig. 2. A schematic of a PEM fuel cell.

catalyst layer and cathode catalyst layer, respectively. Typically, humidified H_2 gas is supplied under pressure into the anode flow channel, which diffuses through the porous electrode until it reaches the anode catalyst layer and forms protons (H^+) and electrons via electrooxidation reaction at the catalyst surface. The protons are transferred through the membrane to the cathode catalyst layer, and the electrons are transported via the external circuit to the cathode. On the other hand, humidified O_2 gas or air is supplied to the cathode flow channel where O_2 gas diffuses through the porous electrode until it reaches the cathode catalyst layer and forms water reacting with protons and electrons, as shown in Fig. 2b. The overall electrochemical reaction occurring in the PEM fuel cell can be represented by the following reaction.

$$H_2 + \frac{1}{2}O_2 \rightarrow 2H_2O + \text{Heat} + \text{Electric Energy} \tag{1}$$

The output electric energy of the fuel cell is calculated from the overall cell voltage (E_{cell}), which can be defined including the combined effect of thermodynamic, mass transport, kinetics, and ohmic resistance as [3]

$$E_{\text{cell}} = E_{\text{oc}} - \eta_{\text{act}} - \eta_{\text{ohm}} \tag{2}$$

In the above equation, E_{oc} is the open circuit potential or voltage at zero current, η_{act} is the losses arising predominantly due to the kinetics at the electrodes, i.e., the catalyst layers, and η_{ohm} represents the losses arising due to the resistive losses in the electrolyte and electrodes. The effect of mass transfer limitation on the cell potential will be incorporated in Section 2.4 explicitly. As seen in Fig. 1, the activation overpotential in the anode catalyst layer is negligible compared to the overpotential in the cathode catalyst layer. Therefore, activation overpotential is considered as potential losses in the cathode catalyst layer only. In an ideal fuel cell, the cell voltage is independent of the current drawn, and the open circuit potential would remain equal to the reversible cell potential (E_{r}). Practically, the ideal cell potential is not possible to attain at the zero current due to another problem for PEM fuel cells, fuel crossover through the membrane, which results in a mixed potential at the cathode and thereby lowers the cell performance [36]. Hence, the following expression is considered for the open circuit potential.

$$E_{\text{oc}} = E_{\text{r}} - E_{\text{mixed}} \tag{3}$$

where E_{mixed} is the mixed potential at the electrodes. This amount of potential drops is mainly due to unavoidable parasitic reactions that tend to lower the equilibrium electrode potential. For instance, it might be due to the crossover of fuel through the electrolyte from anode to cathode or vice versa, slow O_2-reduction kinetics, Pt-oxide formation and/or impurity oxidation, or some other unknown factors.

2.1. Reversible cell potential

The reversible cell voltage (E_{r}) is the cell potential obtained at the thermodynamic equilibrium. For the reaction of the PEM fuel cells shown in Eq. (1), the reversible cell potential can be found from a modified version of the Nernst equation as [3,4,7]

$$E_{\text{r}} = \frac{\Delta G}{2\mathfrak{F}} + \frac{\Delta S}{2\mathfrak{F}}(T - T_{\text{ref}}) - \frac{\mathfrak{R}T}{2\mathfrak{F}} \ln\left(\frac{X_{H_2O}}{X_{H_2} X_{O_2}^{0.5}}\right) + \frac{\Delta N \mathfrak{R} T}{2\mathfrak{F}} \ln\left(\frac{P_{\text{ref}}}{P}\right) \tag{4}$$

where ΔG is the change in Gibbs free energy, $\mathfrak{F}$ is the Faraday's constant (96,487 C mol^{-1}), ΔS is the change in entropy, $\mathfrak{R}$ is the universal gas constant (8.314 J mol^{-1} K^{-1}). The variable T denotes the cell operating temperature, with T_{ref}

denoting a reference temperature (298 K). Similarly, P denotes the operating pressure and P_{ref} denoting reference pressure (1 atm). X_{H_2O}, X_{H_2}, and X_{O_2}, are the mole fraction of water vapor, hydrogen, and oxygen, respectively, and ΔN is the changes in the number of mole in the gas product side and the gas reactant side of Eq. (1). Using the standard-state Gibbs free energy change and entropy change, and considering the product H_2O in the vapor state, Eq. (4) can now be written as

$$E_r = 1.185 - 2.302 \times 10^{-4}(T - T_{\text{ref}}) - 4.308 \times 10^{-5} T \times \ln\left(\frac{X_{H_2O}}{X_{H_2} X_{O_2}^{0.5}}\right) - 2.154 \times 10^{-5} T \ln\left(\frac{P_{\text{ref}}}{P}\right) \quad (5)$$

2.2. Ohmic overpotential

Ohmic overpotential is the total overpotential resulting from the resistance to proton transfer through the membrane and the resistance to electron transfer in the collector plates and the electrodes. Therefore, the total drop in potential due to the ohmic resistance can be defined via an Ohm's law relation as

$$\eta_{\text{ohm}} = \eta_{\text{ohm,p}} + \eta_{\text{ohm,e}} + \eta_{\text{ohm,m}} = R''_{\text{total}} J \quad (6)$$

where R''_{total} is the equivalent of total internal resistance and J is the cell current density. $\eta_{\text{ohm,p}}$, $\eta_{\text{ohm,e}}$, and $\eta_{\text{ohm,m}}$ are the potential drop due to the ohmic resistance of flow channel plate, the electrodes, and membrane layer, respectively. Mathematical formulation for each of these resistances has already been developed [7]. However, careful attention is required to calculate these resistances, since these expressions are dependent on the cell geometry, material properties, and reactant concentration. One can also approximate the total internal resistance from the following empirical relation for typical PEM fuel cell, which is a function of cell temperature and current [28,29]

$$R_{\text{total}} = 0.01605 - 3.5 \times 10^{-5} T + 8.0 \times 10^{-5} I \quad (7)$$

In addition, experimental values of ohmic resistance for PEM fuel cells operating between 50 and 70 °C and 1–5 atm pressure are available in the literature [26]. In the present study, both the empirical relation and the experimental values of the ohmic resistance have been considered to estimate the ohmic overpotential, and specified clearly, before it is being used.

2.3. Activation overpotential

Catalyst layers are the heart of the fuel cell, where electric energy is produced. Among the two activation overpotentials, namely, anode activation overpotential and cathode activation overpotential, anode activation overpotential is negligible compared to the cathode activation overpotential [5,22,27]. Hence, in the following sections, the cathodic overpotential will be referred simply as the activation overpotential neglecting the anodic overpotential and the details of the derivation are also provided here.

2.3.1. Governing equations

In this study, the catalyst layer is assumed as a mixture of Nafion® membrane, supported catalyst and void space. The volume fractions of these components can be varied as can the effective surface area of catalyst that can be characterized by different loadings and catalyst types. The overall reactions in the cathode catalyst layer is taken as

$$O_2 + 4H^+ + 4e^- \rightarrow 2H_2O \quad (8)$$

Assuming the cell is operating in steady state condition and the membrane is fully humidified, the conservation equations for the gas reactants, electron and proton in the cathode catalyst layer can be summarized as follows

$$\text{Reactants: } \nabla \cdot \left(D_i^{\text{eff}} \nabla C_i\right) - \frac{s_i}{nF} \Re_i = 0 \quad (9)$$

$$\text{Electron: } \nabla \cdot \left(\sigma_s^{\text{eff}} \nabla \Psi_s\right) - \Re_i = 0 \quad (10)$$

$$\text{Proton: } \nabla \cdot \left(\sigma_m^{\text{eff}} \nabla \Psi_m\right) + \Re_i = 0 \quad (11)$$

where the subscript i in the above equations represents the reactant species. s_i is a constant equals 2 for H_2, and -1 for O_2, respectively. The superscript "eff" represents the effective transport property values. The effective diffusion coefficient, D_i^{eff}, is calculated using Bruggemann correction from the bulk diffusion coefficient, D_i and the void fraction or porosity, ϕ as

$$D_i^{\text{eff}} = \phi^{3/2} D_i \quad (12)$$

n (=4) in Eq. (9) is the number of electrons transferred in the cathodic reaction [Eq. (8)], and C denotes the concentration of gas species. Ψ_s and Ψ_m in Eqs. (10) and (11) are the electrical potential in the solid electrode and the membrane electrolyte, respectively, and σ_s^{eff} and σ_m^{eff} are the effective conductivities of the solid catalyst and the membrane. $\Re_i$ is the rate of electrochemical reaction, assuming constant proton concentration, is given by the following Butler–Volmer equation

$$\Re_i = A_v J_{0,\text{ref}} \left(\frac{C_i}{C_{i,\text{ref}}}\right)^{\gamma_i} \left\{ \exp\left[\frac{\alpha_a n \mathfrak{F}}{\Re T}(\Psi_s - \Psi_m)\right] - \exp\left[-\frac{\alpha_c n \mathfrak{F}}{\Re T}(\Psi_s - \Psi_m)\right] \right\} \quad (13)$$

Here A_v is the catalyst reactive surface area per unit volume, $J_{0,\text{ref}}$ is the reference current density at the reference concentration of $C_{i,\text{ref}}$, γ_i is the overall reaction order with respect to the reactant species i, α_a and α_c are the apparent transfer coefficient for the anodic and cathodic reactions, respectively, and $(\Psi_s - \Psi_m)$ represents the activation overpotential (η_{act}) which is the driving force for electrochemical reactions.

2.3.2. One-dimensional formulation

Considering the cathode catalyst layer is a matrix of Pt-catalyst, Nafion® membrane electrolyte and void space, as

shown schematically in Fig. 2, and the spatial coordinate x is defined in Fig. 2b, with the positive direction pointing from the membrane and catalyst layer (CL) interface toward the gas diffusion layer (GDL). Since the thickness of the cathode catalyst layer is almost 4–5 order of magnitude smaller than the cell height, therefore Eqs. (9)–(11) can be simplified as a first approximation in one dimension for constant $D_{O_2}^{eff}$, σ_s^{eff}, and σ_m^{eff} as

$$\frac{d^2 C_{O_2}}{dx^2} = \frac{s_i}{n\mathfrak{F} D_{O_2}^{eff}} \Re_i \tag{14}$$

$$\frac{d^2 \Psi_s}{dx^2} = \frac{\Re_i}{\sigma_s^{eff}} \tag{15}$$

$$\frac{d^2 \Psi_m}{dx^2} = -\frac{\Re_i}{\sigma_m^{eff}} \tag{16}$$

where σ_s^{eff} and σ_m^{eff} are calculated with Bruggemann correction from the bulk conductivity using following expressions

$$\sigma_s^{eff} = \sigma_s (1 - \phi_c)^{3/2} \tag{17}$$

$$\sigma_m^{eff} = \sigma_m (l_m \times \phi_c)^{3/2} \tag{18}$$

and $D_{O_2}^{eff}$ using Eq. (12). Here, l_m denotes the volume fraction of the membrane in the catalyst layer void region, σ_s and σ_m are the bulk conductivities of the solid catalyst and the membrane, respectively, and ϕ_c is the void fraction of the catalyst layer. The void fraction of the catalyst layer is calculated from the known values of catalyst loading (f_{Pt}), the catalyst layer thickness (δ_c) and the densities of platinum and carbon black (ρ_{Pt} and ρ_c) as

$$\phi_c = 1 - \left(\frac{1}{\rho_{Pt}} + \frac{1 - f_{Pt}}{f_{Pt}\rho_c} \right) \frac{m_{Pt}}{\delta_c} \tag{19}$$

Furthermore, the potential drop across the cathode catalyst layer is defined as $\eta_{act} = \Psi_s - \Psi_m$, hence it can be written as

$$\frac{d^2 \eta_{act}}{dx^2} = \frac{d^2 \Psi_s}{dx^2} - \frac{d^2 \Psi_m}{dx^2} \tag{20}$$

also combining Eqs. (15) and (16) yields

$$\sigma_s^{eff} \frac{d^2 \Psi_s}{dx^2} = -\sigma_m^{eff} \frac{d^2 \Psi_m}{dx^2} \tag{21}$$

Typically, the electrical conductivity in the conducting solid (σ_s^{eff}) is several orders of magnitude larger than the conductivity of the membrane phase (σ_m^{eff}). Therefore, it can be immediately recognized from the above equation that the second order derivative of the potential in the solid phase will be very small compared to the second order derivative of the membrane phase potential. Combining Eqs. (13), (16), and (20) yields

$$\frac{d^2 \eta_{act}}{dx^2} = \frac{A_v J_{0,ref}}{\sigma_m^{eff}} \left(\frac{C_{O_2}}{C_{O_2,ref}} \right)^{\gamma_i} \left\{ \exp\left[\frac{\alpha_a n \mathfrak{F} \eta_{act}}{\Re T} \right] - \exp\left[-\frac{\alpha_c n \mathfrak{F} \eta_{act}}{\Re T} \right] \right\} \tag{22}$$

Table 1
Catalyst surface areas as a function of the fraction of Pt-catalyst [38]

Catalyst type	f_{Pt}	A_s (m^2/g)
Pt on carbon black	0.1	140
	0.2	112
	0.3	88
	0.4	72
	0.6	32
	0.8	11
Pt black	1.0	28

Above equation describes the electrochemical reaction in the cathode catalyst layer, where C_{O_2} represents the oxygen concentration in the cathode catalyst layer. The reference current density ($J_{0,ref}$) is calculated using the experimental data of Parthasarathy et al. [37] and the reference oxygen concentration, $C_{O_2,ref}$ corresponding to $J_{0,ref}$ is taken as 12 mol/m^3 [7,37]. The experimental data of the reference exchange current density in A/cm^2 for oxygen reduction in Nafion® were correlated with the cell temperature in Kelvins by the following relation [22]

$$\log_{10}(J_{0,ref}) = 3.507 - \frac{4001}{T} \tag{23}$$

The specific reaction surface (A_v) is derived from the catalyst mass loading per unit area of cathode (m_{Pt}), catalyst surface area per unit mass of the catalyst (A_s), and catalyst layer thickness (δ_c) by the following relation [22]

$$A_v = \frac{A_s m_{Pt}}{\delta_c} \tag{24}$$

Here the catalyst surface area per unit mass of the catalyst is a function of the fraction of the Pt-catalyst on the carbon support (f_{Pt}). Typical values of the catalyst surface area as a function of the amount of Pt-loading is shown in Table 1.

2.3.3. Exact solution of activation overpotential

Neglecting the concentration overpotential, assuming the concentration of oxygen in the cathode catalyst layer is constant and $\alpha_a = \alpha_c = \alpha$, Eq. (22) can be simplified as

$$\frac{d^2 \eta_{act}}{dx^2} = \kappa' \sinh\left(\frac{\alpha n \mathfrak{F} \eta_{act}}{\Re T} \right) \tag{25}$$

where κ' is a constant. Furthermore, considering the following scaled variables, scaled thickness of the catalyst layer (X) and scaled activation overpotential ($\bar{\eta}_{act}$)

$$X = \frac{x}{\delta_c} \tag{26}$$

$$\bar{\eta}_{act} = \frac{\alpha n \mathfrak{F} \eta_{act}}{\Re T} \tag{27}$$

Eq. (25) is written in scaled form as

$$\frac{d^2 \bar{\eta}_{act}}{dX^2} = \boldsymbol{\kappa} \sinh(\bar{\eta}_{act}) \tag{28}$$

where the dimensionless parameter κ is defined by the following relation

$$\kappa = \frac{A_v J_{0,\mathrm{ref}}}{\sigma_m^{\mathrm{eff}}} \left(\frac{C_{O_2}}{C_{O_2,\mathrm{ref}}}\right)^{\gamma_i} \frac{2\alpha n \mathfrak{F} \delta_c^2}{\Re T} \tag{29}$$

Scaled form of the governing equation for the activation overpotential (Eq. (28)) is a second order non-linear equation, which can be solved analytically for appropriate boundary conditions. The steps of the analytical solution along with the boundary conditions are given below. The exact solution of Eq. (28) can be obtained by multiplying both side by $\frac{d\bar{\eta}_{act}}{dX}$ and integrating twice as follows.

$$\frac{d}{dX}\left[\left(\frac{d\bar{\eta}_{act}}{dX}\right)^2\right] = 2\kappa \sinh(\bar{\eta}_{act}) \frac{d\bar{\eta}_{act}}{dX} \tag{30a}$$

$$\frac{d\bar{\eta}_{act}}{dX} = \pm\sqrt{2\kappa \cosh(\bar{\eta}_{act}) + C_1} \tag{30b}$$

It is noticed that the gradient of the membrane potential on the interface between the catalyst layer and the gas diffusion layer is zero. In addition, if the membrane potential at $x = \delta_c$ is considered as the reference potential then the following boundary conditions are available.

$$\frac{d\bar{\eta}_{act}}{dX} = 0 \quad \text{at} \quad x = \delta_c \tag{31a}$$

$$\bar{\eta}_{act} = 0 \quad \text{at} \quad x = \delta_c \tag{31b}$$

Applying these boundary conditions in Eq. (30b), the integration constant C_1 is found as -2κ. Also $\frac{d\bar{\eta}_{act}}{dX}$ has to be negative to satisfy second boundary condition, hence

$$\frac{d\bar{\eta}_{act}}{dX} = -\sqrt{2\kappa[\cosh(\bar{\eta}_{act}) - 1]} \tag{32}$$

To obtain the relation between the current density and the overpotential, another boundary condition is required that is specified as

$$\sigma_m^{\mathrm{eff}} \frac{d\Psi_m}{dx} = J \quad \text{at} \quad x = 0 \tag{33}$$

where J is the total current density drawn from the cell. Using Eq. (33) in Eq. (32), the exact solution of the activation overpotential for PEM fuel cell is obtained as

$$J = \frac{\Re T \sigma_m^{\mathrm{eff}}}{\alpha n \mathfrak{F} \delta_c} \sqrt{2\kappa\left[\cosh\left(\frac{\alpha n \mathfrak{F} \eta_{act}}{\Re T}\right) - 1\right]} \tag{34}$$

Once again, this expression of activation overpotential represents only the cathodic overpotential, and is obtained by assuming no variation of oxygen concentration in the cathode catalyst layer of PEM fuel cell and equal transfer coefficients in the Butler–Volmer equation. Since all the parameters are known for a specific fuel cell except oxygen concentration in the catalyst layer, it can easily be estimated by knowing the oxygen concentration. In the following subsection, an approximate formulation to calculate the oxygen concentration is described.

2.4. Calculation of oxygen concentration

For fully hydrated membrane in the cathode catalyst layer, the concentration of proton at the reaction sites is fixed and constant, and its specific value depends on the type of the membrane used. Conversely, the concentration of oxygen depends on the rate of electro-chemical reaction or current density, as well as diffusion through the electrode and liquid water layer. Also concentration within the catalyst layer varies with the distance from the electrode–catalyst layer interface. For small current densities, the concentration variation is very small. At intermediate and high current densities, concentration of oxygen decays sharply within a small region in the catalyst layer near the catalyst layer–GDL interface [22]. Since the region of the catalyst layer where electro-chemical reactions occurs, is very small; it can be assumed that the oxygen concentration is constant in that small region and independent of length scale x in the cathode catalyst layer. Unlike Marr and Li [22], it is considered that oxygen concentration at $x = 0$ is known but depends on the current density. This will eventually provide better approximation of O_2 concentration than the estimates of Marr and Li [22]. In the following two subsections, the details of the oxygen concentration calculations in the catalyst layer and on the catalyst surface are provided.

2.4.1. Flooded electrode

During the transport process, O_2 in the flow channels first convects to the surface of the electrode, and then diffuses through the electrode to the catalyst layer surface as shown in Fig. 3. Considering a uniform oxygen concentration in the cathode flow channel (C_{ch}), the average concentration at the surface of the electrode (C_{es}) can be defined as a function of current density by [7]

$$C_{es} = C_{ch} - \frac{d_h W L}{4Sh\mathfrak{F} D_{O_2,\mathrm{bulk}} A_c} J \tag{35}$$

Here d_h is the hydraulic diameter of the flow channel, W is the width of the cell, L is the length of the cell, $D_{O_2,\mathrm{bulk}}$ represents the diffusion coefficient of oxygen in the gas mixture of the flow channel, and A_c is the area of the flow channels exposed to the electrode. In the above equations, the Sherwood number is denoted by Sh, and due to the laminar

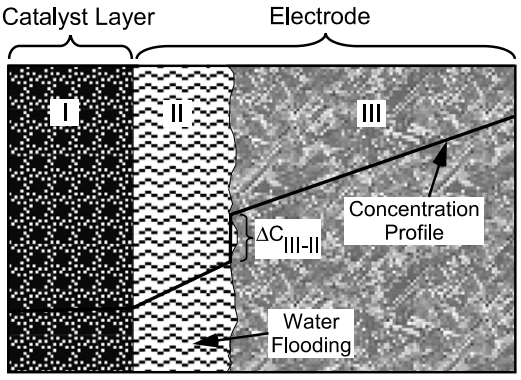

Fig. 3. Schematic profile of oxygen concentration in the partially flooded electrode and cathode catalyst layer.

flow in the flow channels, is equal to 2.3. The bulk diffusion coefficient is calculated according to [39]

$$D_{O_2,bulk} = \frac{1 - X_{O_2}}{\frac{X_{N_2}}{D_{O_2-N_2}} + \frac{X_{H_2O}}{D_{O_2-H_2O}}} \tag{36}$$

where X_{O_2}, X_{N_2} and X_{H_2O} are the mole fractions of oxygen, nitrogen and water vapor in the flow channel, respectively. The binary diffusion coefficient of oxygen and nitrogen, $D_{O_2-N_2}$, is calculated using Chapman–Enskog formula [39] and the binary diffusion coefficient of oxygen and water vapor, $D_{O_2-H_2O}$, is calculated using Slattery–Bird equation [40] as described in Appendix A.

Once the concentration on the surface of the electrode is known, the oxygen concentration on the other side of the electrode (at the interface with liquid water in Fig. 3) is estimated using the Fick's law of diffusion

$$C_{III-II} = C_{es} - N''_{O_2} R_{III} \tag{37}$$

where R_{III} is the resistance to mass transfer caused by the oxygen diffusion through the electrode and N''_{O_2} is the molar flux of oxygen and is defined by

$$N''_{O_2} = \frac{J}{4\mathfrak{F}} \tag{38}$$

At the interface of liquid water and electrode, oxygen concentration is further reduced due to the limitation of transport processes in the liquid medium. Since the oxygen is weakly soluble in liquid water under the typical fuel cell operating environment, the amount of concentration drop at the liquid–gas interface can be related by using the perfect gas law and Henry's law as

$$\Delta C_{III-II} = C_{III-II}\left(1 - \frac{\mathfrak{R}T}{H_{O_2}}\right) \tag{39}$$

where H_{O_2} is Henry's constant for oxygen gas dissolution in liquid water, which may be determined from the empirical correlation given below [5]

$$H_{O_2} = 0.1013 \exp\left(14.1 - \frac{666}{T}\right) \tag{40}$$

where the temperature T is in Kelvins, and H_{O_2} is in the unit of Pa m^3/mole.

Although practically the thickness of the water flooding layer is non-uniform, in the present investigation the thickness of the liquid water in the electrode is considered uniform, consistent with the present 1-D analysis. Hence, the decay of oxygen concentration in the liquid water layer is approximated using the Fick's law formulation as Eq. (37)

$$C_{II-I} = (C_{III-II} - \Delta C_{III-II}) - N''_{O_2} R_{II} \tag{41}$$

where R_{II} is the resistance to mass transfer caused by the oxygen dissolving into the liquid water. Considering f_w is the fraction of the void region in the electrode that is flooded by liquid water, both the resistances (R_{II} and R_{III}) are expressed by the volume fraction divided by the corresponding diffusion coefficient

$$R_{II} = \frac{f_w \delta_e}{D^{eff}_{O_2-H_2O_{(l)}}} \tag{42}$$

$$R_{III} = \frac{(1 - f_w)\delta_e}{D^{eff}_{O_2,bulk}} \tag{43}$$

Here δ_e is the electrode thickness. $D^{eff}_{O_2-H_2O_{(l)}}$ and $D^{eff}_{O_2,bulk}$ are the effective diffusion coefficients of oxygen through the liquid water zone and the gas zone in the electrode as shown in Fig. 3. Both of these effective diffusion coefficients are evaluated from their bulk values using Eq. (12) with the porosity equal to the electrode porosity (ϕ_e). The binary diffusion coefficient of oxygen in liquid water ($H_2O_{(l)}$) is obtained using Wilke–Chang equation [39] as described in Appendix A. Combining Eqs. (37)–(39), and (41) yields

$$C_{II-I} = C_{es}\frac{\mathfrak{R}T}{H_{O_2}} - \frac{J}{4\mathfrak{F}}\left(R_{II} + R_{III}\frac{\mathfrak{R}T}{H_{O_2}}\right) \tag{44}$$

It should be noted here that the concentration given by Eq. (44) is valid only when $f_w > 0$. The concentration further drops down before reaching the catalyst particles, i.e., at the surface of the catalyst particles, actual oxygen concentration is slightly lower than the above-mentioned concentration. Since the actual composition of the catalyst layer is more complex and not available in the literature, one may neglect the composition effect and assume the constant concentration profile in the cathode catalyst layer using Eq. (44). In the present investigation, uniform concentration profile is considered in the catalyst layer, which is equal to the concentration at the interface of the electrode and the catalyst layer, i.e., $C_{O_2,CL} = C_{II-I}$. However, to study the effect of the Nafion® content in the catalyst layer and water flooding, it is required to consider the oxygen concentration on the catalyst particle's surface. Considering the catalyst particles are surrounded by Nafion® membrane and water layer, the oxygen concentration on the surface of the catalyst particle is approximated by applying the Fick's law

$$C_{O_2,catalyst} = C_{II-I} - \frac{J}{4\mathfrak{F}}(R_{w,c} + R_{m,c}) \tag{45}$$

where $R_{w,c}$ and $R_{m,c}$ represent the resistance to mass transfer in the liquid water and the resistance to mass transfer in the membrane content of the cathode catalyst layer, respectively. If the electrode is assumed partially flooded, then the catalyst layer would be fully flooded, and the resistances can be determined as

$$R_{w,c} = \frac{l_{H_2O}\delta_c}{D^{eff}_{O_2-H_2O_{(l)},c}} \tag{46}$$

$$R_{m,c} = \frac{l_m \delta_c}{D^{eff}_{O_2-m,c}} \tag{47}$$

where l_{H_2O} and l_m are the volume fraction of liquid water and membrane in the void region of the catalyst layer, respectively. The effective diffusion coefficients of oxygen through the water and the Nafion® membrane in the void region of the catalyst layer are denoted by $D^{eff}_{O_2,H_2O_{(l)},c}$ and $D^{eff}_{O_2-m,c}$,

respectively. These effective values are again related to the bulk values by the Bruggemann's correction

$$D^{\text{eff}}_{\text{O}_2\text{–H}_2\text{O}_{(l)},c} = \phi_c^{3/2} D_{\text{O}_2\text{–H}_2\text{O}_{(l)}} \tag{48}$$

$$D^{\text{eff}}_{\text{O}_2\text{–m,c}} = \phi_c^{3/2} D_{\text{O}_2\text{–m}} \tag{49}$$

and the diffusion coefficient for oxygen in Nafion® membrane ($D_{\text{O}_2\text{–m}}$) is calculated using the empirical relation [22] given in Appendix A.

2.4.2. Dry electrode

Formulation given in the above section is valid only when the electrode is flooded as shown in Fig. 3. For dry electrode ($f_w = 0$), zone II does not exist in Fig. 3. Then the oxygen concentration at the interface of the electrode and catalyst layer is calculated directly using the Fick's law as

$$C_{\text{III–I}} = C_{\text{es}} - \frac{J}{4\mathfrak{F}} R_{\text{III}} \tag{50}$$

Since un-flooded electrode is considered, which means catalyst particles are no longer completely surrounded by the Nafion® and water. In this circumstance, there will be some void space over the catalyst particle that is filled with gas mixture. Therefore, oxygen has to penetrate three layers, namely, Nafion® membrane, liquid water, and gas mixture layer. In reality, it can be more than three layers as mentioned, it can be any combinations of the Nafion®, water, and gases. However, for simplification it has been considered that catalyst particles are surrounded by three distinct layers of Nafion®, water, and gas. Hence, the following resistance for the mass transfer associated with the gas mixture in the partially flooded catalyst layer is formulated along with Eqs. (46) and (47) for the liquid water and the Nafion® membrane

$$R_{\text{g,c}} = \frac{(1 - l_{\text{m}} - l_{\text{H}_2\text{O}})\delta_c}{D^{\text{eff}}_{\text{O}_2\text{,gas,c}}} \tag{51}$$

where $D^{\text{eff}}_{\text{O}_2\text{,gas,c}}$ is the effective diffusion coefficients of oxygen through the gas and expressed as

$$D^{\text{eff}}_{\text{O}_2\text{,gas,c}} = \phi_c^{3/2} D_{\text{O}_2\text{,bulk}} \tag{52}$$

Similar to the formulation of Eqs. (44) and (45), the expression for the oxygen concentration on the catalyst particle surfaces for the partially flooded catalyst layer is written as

$$C_{\text{O}_2\text{,catalyst}} = C_{\text{II–I}} \frac{\Re T}{\text{H}_{\text{O}_2}} - \frac{J}{4\mathfrak{F}} \left(R_{\text{g,c}} \frac{\Re T}{\text{H}_{\text{O}_2}} + R_{\text{w,c}} + R_{\text{m,c}} \right) \tag{53}$$

3. Results and discussion

In this section, a comparison between the present model predictions with the results available in the literature is provided [26–28,41]. Although the analytical solution provided here is mathematically "exact", the comparison will provide an idea how accurate is the assumption made during the derivation process. Following this, the effect of operating conditions on the cell performance and results of an optimization study using the analytical activation overpotential formulation are provided.

3.1. Model comparison

Here a wide range of comparison has been covered that includes comparison with the empirical correlations [26], comparison with the experimental data [28,41], and comparison with the numerical predictions [27] as provided in the following subsections.

3.1.1. Comparison with empirical correlations

In the first set of comparison, the empirical correlation provided by Kim et al. [26] is used to generate empirical results. Two different sets of reactant gases were considered in their correlations. In the first set, air is used as the cathode gas and hydrogen as the fuel, and in the second set, oxygen is used as the cathode gas and hydrogen as the fuel. In their empirical correlations, the experimental results were curve-fitted with an empirical equation for a PEM fuel cell with distinct terms of open circuit potential, activation overpotential, and ohmic overpotential. This empirical correlation eventually allowed us to incorporate their experimental estimates of ohmic resistance to obtain the total cell polarization. In addition, Kim et al. [26] provided another empirical relation that included mass-transport overpotential as an exponential function of the current density. The mass-transport overpotential is significant at higher current densities, particularly at close to the limiting current density. For comparison purpose, mass-transport term is also incorporated with one set of present model data. Finally, the cell voltage is calculated using the following relation, with the activation overpotential derived in Section 2.3.3.

$$E_{\text{cell}} = E_r - \frac{\Re T}{\alpha n \mathfrak{F}} \cosh^{-1}\left[\frac{1}{2\kappa} \left(\frac{\alpha n \mathfrak{F} J \delta_c}{\Re T \sigma_m^{\text{eff}}} \right)^2 + 1 \right] - R''_{\text{total}} J - a \exp(bJ) - E_{\text{mixed}} \tag{54}$$

Fig. 4 depicts a comparison of the total polarization obtained in the present study with the corresponding empirical results of Kim et al. [26] for air as the cathode gas in part (a), and oxygen as the cathode gas in part (b). Here, both lines represent the results of the present investigation for cell operating at 1 atm of pressure and 70 °C; and symbols represent the corresponding experimental results. For both cases (with mass-transport overpotential and without mass-transport overpotential), the total cell potential is calculated using the identical parameters as provided in the literature with appropriate water flooding parameters [7]. The ohmic overpotential and the mass-transport overpotential are obtained directly using the equivalent internal ohmic resistance (R''_{total}) and coefficients of mass-transport (a and b in Eq. (54)). These values can be found in the literature, and the cell design parameters used in the model are listed in Table 2. The comparison with the empirical

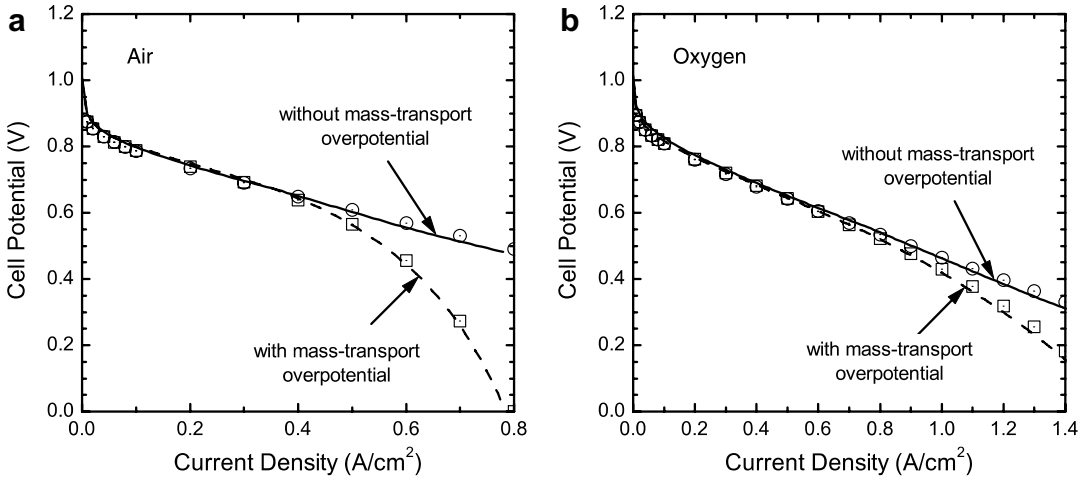

Fig. 4. Comparison of the present analytical estimates of the cell polarization operating at 1 atm and 70 °C with the experimental data of Kim et al. [26] for (a) air as the cathode gas and hydrogen as the anode gas, and (b) oxygen as the cathode gas and hydrogen as the anode gas. Lines represent the analytical results of the present investigation whereas symbols represent the experimental results for without mass-transport overpotential and with mass-transport overpotential as indicated in the figure.

Table 2
Parameters used to model the data from Kim et al. [26]

Parameter	Value
Width of the cell, W (cm)	7.07
Length of the cell, L (cm)	7.07
Electrode thickness, δ_e (μm)	250
Catalyst layer thickness for O_2 as the cathode gas, δ_c (μm)	12.3
Catalyst layer thickness for Air as the cathode gas, δ_c (μm)	0.26
Void fraction of the cathode electrode, ϕ_e	0.4
Fraction of membrane in the cathode catalyst layer for O_2 as the cathode gas, l_m	0.4
Fraction of membrane in the cathode catalyst layer for Air as the cathode gas, l_m	0.1
Catalyst loading per unit area, m_{Pt} (mg/cm^2)	0.3
Fraction of platinum on carbon support for O_2 as the cathode gas, f_{Pt}	0.2
Fraction of platinum on carbon support for Air as the cathode gas, f_{Pt}	1
Mixed electrode potential for 1 atm of pressure, E_{mixed} (V)	0.17
Mixed electrode potential for 5 atm of pressure, E_{mixed} (V)	0.16

results for cell operating condition of 5 atm of pressure and 70 °C is illustrated in Fig. 5. All parameters are the same as in Fig. 4 except the water flooding parameter, which is taken from Baschuk and Li [7] for the 5 atm and 70 °C.

The model results presented in Figs. 4 and 5 show that there is an excellent agreement between the empirical data and the estimates of the analytical model when water flooding of the cathode electrode is incorporated, particularly at intermediate current densities. In all the cases, cell potential is slightly overestimated by the analytical model at lower current densities when $J < 0.1$ A/cm^2. Whereas cell potential is slightly underestimated at higher current densities ($J > 0.6$ A/cm^2 for air and $J > 1.0$ A/cm^2 for oxygen). This is probably due to the assumption made for the analytical formulation. Here a constant oxygen concentration is assumed in the catalyst layer, which is giving lower activation overpotential in the cathode catalyst layer. Also the mixed electrode potential in the analytical model is estimated by matching the ohmic resistances at the intermediate current density. It has been found that the mixed electrode potential is approximately 0.17 V for 1 atm pressure and 70 °C, and 0.16 V for 5 atm pressure and 70 °C. It should also be noted here, the water flooding data are not available for the low current densities and zero flooding has been assumed for those cases. This is also a reason for the slight overestimation of the cell potential at low current densities. On the other hand, Kim et al. [26] reported various open circuit voltages, which imply various mixed electrode potentials involved in their experiments. In the present model, only the cathodic activation overpotential has been considered along with the ohmic overpotential and iterative estimates of mixed electrode potential. The anodic overpotential has been neglected, which might be another reason for this slight overestimation. Furthermore, at higher current densities, the estimated oxygen concentration is lower than the real cell's concentration as only one dimensional linear decay of oxygen profile has been considered. Oxygen concentration might not decay that rapidly in the test fuel cell due to the 3-D distribution of the liquid water in the electrode. Hence higher activation overpotential has been estimated for large current densities and lower cell potential. Nevertheless, these comparisons reveal the robustness of the present analytical formulation.

3.1.2. Comparison with experimental data

In the second set of comparison, the present model predictions are compared with the experimentally determined cell performance data. Figs. 6 and 7 show the comparison between the model predictions and the experimental results of Ballard's BAM® Composite fuel cell [41] and Ballard Mark® IV fuel cell [28], respectively. The Ballard BAM® Composite cell data were from a cell being operated at 3.02 bara pressure, 80 °C and using air as the oxidant.

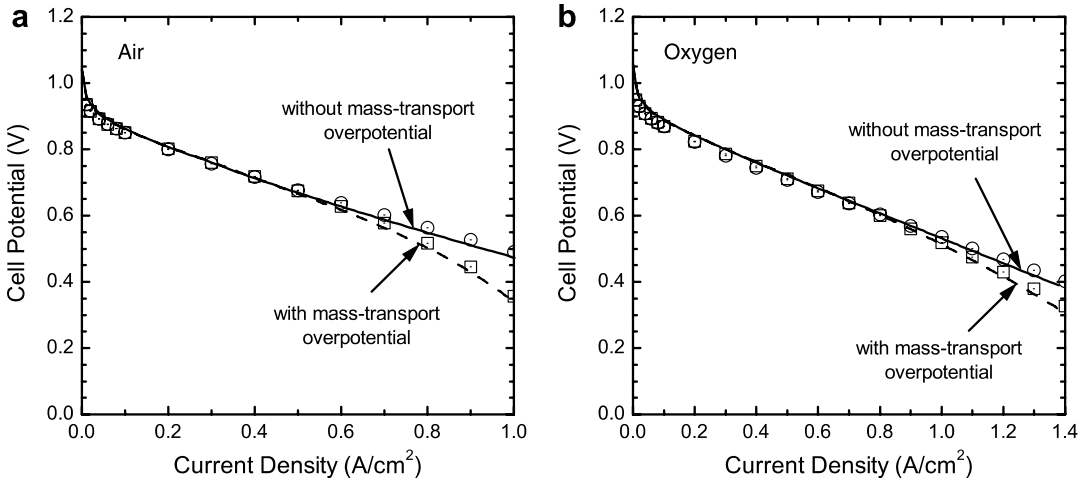

Fig. 5. Comparison of the present analytical estimates of the cell polarization operating at 5 atm and 70 °C with the experimental data of Kim et al. [26] for (a) air as the cathode gas and hydrogen as the anode gas, and (b) oxygen as the cathode gas and hydrogen as the anode gas. Lines represent the analytical results of the present investigation whereas symbols represent the experimental results for without mass-transport overpotential and with mass-transport overpotential as indicated in the figure.

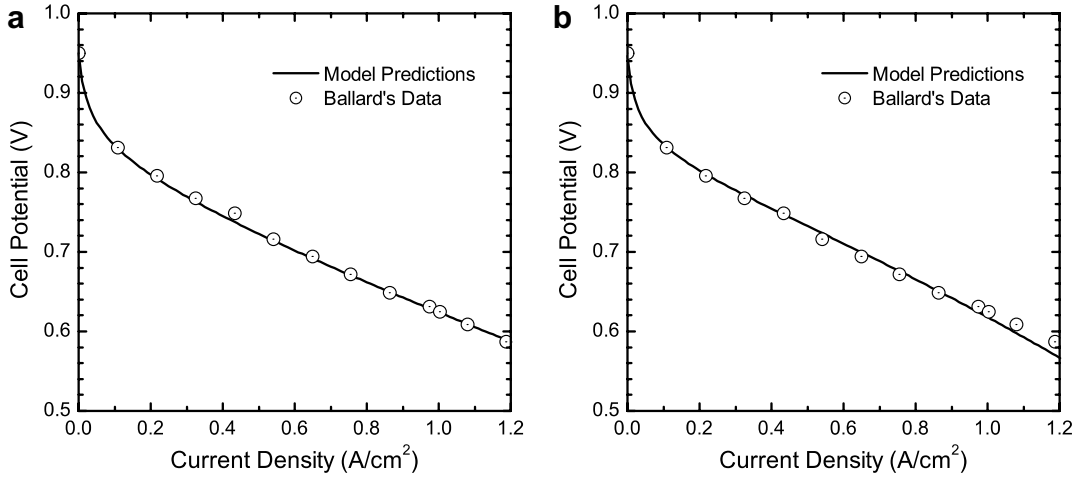

Fig. 6. Comparison between the present analytical predictions and the experimental results of Ballard's BAM® Composite cell operating at 3.02 bar and 80 °C for air as the cathode gas and hydrogen as the anode gas [41] for two types of ohmic resistances (a) constant ohmic resistance, and (b) variable ohmic resistance calculated using Eq. (7) taken from [28,29] originally developed for Mark® IV fuel cells.

The Ballard Mark® IV fuel cell system data were taken from a cell operating at 30 psig pressure, 70 °C and using oxygen as the oxidant. The cell design parameters used for fitting these experimental data are listed in Table 3. For the Ballard BAM® Composite cell data, two techniques in ohmic overpotential calculation have been considered. In Fig. 6a, the ohmic resistance is estimated directly from the slope of the experimental polarization curve; whereas in Fig. 6b, the total internal ohmic resistance is obtained using Eq. (7) taken from [28,29] originally developed for the Mark® IV fuel cells. Both sets of the model predictions and the experimental results show good agreement like the empirical results shown in the previous section. The empirical formulation for internal ohmic resistance provides a slight underestimation of the cell potential for higher current densities (Fig. 6b). This underestimation could easily be explained by comparing the ohmic resistance variations with current density, as ohmic resistance is higher for higher current density in Fig. 6b compared to the ohmic resistance in Fig. 6a. The ohmic resistance in Fig. 7 is considered as constant and calculated directly from the experimental data. For illustration purpose, the activation polarization curve is also included in Fig. 7. It has been seen that the present model also agrees with Mark® IV fuel cell data, like the comparison with Ballard BAM® Composite cell.

3.1.3. Comparison with numerical results

Fig. 8 demonstrates the comparison between the present model predictions and the numerical results of Rowe and Li [27] for a PEM fuel cell running with 3 atm and 80 °C air as the cathode gas and hydrogen as the anode gas.

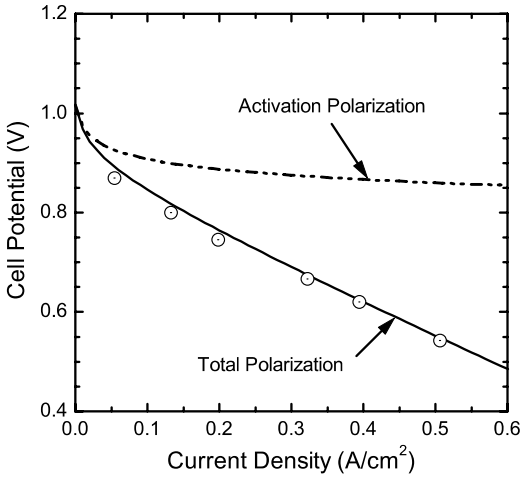

Fig. 7. Comparison between the present analytical predictions with the experimental results of Ballard Mark® IV fuel cell system operating at 70 °C using 30 psig H_2 and 30 psig O_2 [28].

Table 3
Cell design parameter used to model Ballard BAM® Composite cell and Ballard Mark® IV cell data

Parameter	Value	
	BAM®	Mark® IV
Electrode thickness, δ_e (μm)	200	200
Catalyst layer thickness, δ_c (μm)	10	10
Void fraction of the cathode electrode, ϕ_e	0.4	0.4
Fraction of membrane in the cathode catalyst layer, l_m	0.65	0.4
Catalyst loading per unit area, m_{Pt} (mg/cm^2)	0.332	0.3
Fraction of platinum on carbon support, f_{Pt}	0.4	0.2
Mixed electrode potential, E_{mixed} (V)	0.243	0.189

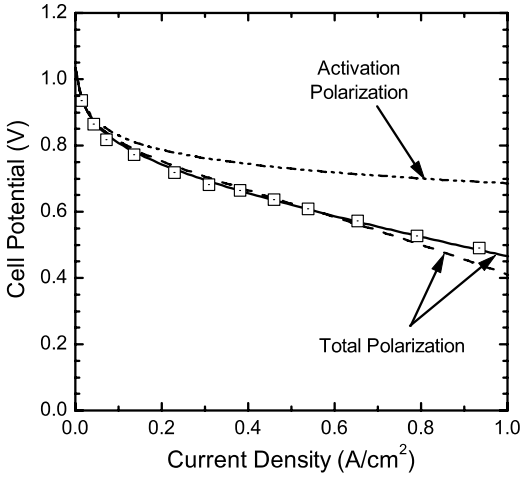

Fig. 8. Polarization curve estimated by the present analytical model with the numerical model of Rowe and Li [27] for a PEM fuel cell operating at 3 atm and 80 °C with air as the cathode gas. Solid line represents the analytical polarization curve for constant ohmic overpotential, the dashed line is for variable ohmic overpotential (using Eq. (7)), and symbols represent the numerical results of Rowe and Li [27]; whereas dashed-dot-dot line shows the corresponding activation polarization curve.

Table 4
Parameters used to model the data of Rowe and Li [27]

Parameter	Value
Electrode thickness, δ_e (μm)	200
Catalyst layer thickness, δ_c (μm)	7
Void fraction of the cathode electrode, ϕ_e	0.4
Fraction of membrane in the cathode catalyst layer, l_m	0.45
Catalyst layer flooding (%)	99
Fraction of catalyst, f_{Pt}	0.2
Specific reaction surface area, A_v (cm^2/cm^3)	1×10^5
Reference current density, $J_{0,ref}$ (A/cm^2)	9.5×10^{-8}
Membrane conductivity, σ_m (S/cm)	0.15
Mixed electrode potential for 1 atm of pressure, E_{mixed} (V)	0.158

Using the parameter values listed in Table 4, the predicted polarizations based on the analytical formulation are compared with the numerical data for 20 wt.% Pt/C catalyst loading. The solid line depicts the total polarization curve for constant ohmic overpotential, and the dashed line represents the total polarization with variable ohmic overpotential (using Eq. (7)), whereas the dashed-dot-dot line shows the corresponding activation polarization curve. Here symbols are showing the numerical predictions of Rowe and Li [27]. It is seen from this comparison that the proposed analytical model is also capable of producing the identical results of numerical model developed earlier in the literature. Both the constant ohmic overpotential case and the variable ohmic overpotential results agree well with the numerical result up to $J \leqslant 0.6$ A/cm^2. Once again, variable ohmic overpotential model underestimates the cell potential for large current densities like Fig. 6b. Unlike Fig. 7, here more common trend has been noticed in the cell polarization that the activation overpotential is larger than the ohmic overpotential.

The results provided in the previous three sub-sections give a considerable insight about the proposed analytical model and its robustness. It should also be noted that no adjustment to the reactive surface area, A_v, or the exchange current density, $J_{0,ref}$, is required to achieve the level of agreement shown in Figs. 4–8 as all the parameter values were taken directly from the literature. However, results shown in Section 3.1.2 for the comparison with the experimental results, the reactive surface area, A_v, or the exchange current density, $J_{0,ref}$, have been assumed similar to the value used in Fig. 4 as no such data were reported by Amphlett et al. [28]. In addition, fraction of Pt-loading in the catalyst layer has also been assumed in modeling the experimental results due to missing information in the literature. However, the model predictions have been tested by changing the fraction of Pt-loading, and that does not show any significant effect on the total cell polarization. For instance, in Ballard BAM® composite fuel cell changing the f_{Pt} between 0.3 and 0.5 provides almost identical results as shown in Fig. 6. The only parameter that has been adjusted during these comparisons is the mixed electrode potential (E_{mixed}). Even for Ballard BAM® composite fuel cell, it has been observed that without using Eq. (3)

one can generate identical results of Ballard's experimental results by taking $E_{oc} = E_{cell}$ for $J \to 0$ from their experimental curve. Also noted here, the adjustment on the mixed electrode potential does not change the behavior of the polarization curve as E_{mixed} is independent of cell parameters as well as independent of current density. Hence, the analytical formulation can be used in the performance and optimization study with proper ohmic overpotential formulation avoiding complicated numerical computations or expensive experiments to predict the polarization of PEM fuel cell. Moreover, this method is not only as simple as shown in Eq. (34) but also as accurate as experimental predictions.

3.2. Cell performance and optimization

A comprehensive comparison of the present analytical model predictions with the various data available in the literature has already been provided in the previous section. In this section, a performance and optimization analysis will be carried out based on the analytical formulation developed in this study. In the following section, the results are given using the analytical expression given in Eq. (34) and the ohmic overpotential is calculated using the ohmic resistance given by Eq. (7) in all subsequent results.

3.2.1. Effect of the operating conditions

Fig. 9 depicts the effect of operating temperature on the cell potential for air as the cathode gas (Fig. 9a), and oxygen as the cathode gas (Fig. 9b). Here an un-flooded electrode and fully-flooded catalyst layer has been considered to model these results. Detailed description of the base case operating and physical parameters used in the present model calculations are given in Table 5. The present model predictions show almost negligible temperature effect on the cell polarization curve for both air and oxygen based fuel cells. However at large current densities, a slight increase in cell potential is observed as temperature is increased. For instance, at $J = 0.8$ A/cm^2 cell potential is about 10 mV higher for 80 °C compared to the cell potential at 50 °C. Ideally, the cell polarization decreases with an increase in the cell operating temperature due to better electrochemical reaction at higher temperatures. Here only small difference has been observed since the reversible cell potential decreases with the temperature as well. However, Ballard Power Systems suggest that there is approximately a 30% increase in cell potential when the temperature is increased from 30 °C to 80 °C, no such improvement has been observed here like Marr and Li [25]. This is largely due to the fully-flooded catalyst layer, where temperature has less effect on the cell potential than the partially flooded catalyst layer.

A better explanation of such temperature effect might be possible by investigating the response of the activation

Table 5
Base case operating and physical parameters used in the present model calculations

Parameter	Value
Operating temperature, T (°C)	80
Operating pressure, P (atm)	3
Length of the cell, L (cm)	5
Width of the cell, W (cm)	5
Electrode thickness, δ_e (μm)	250
Catalyst layer thickness, δ_c (μm)	10
Void fraction of the cathode electrode, ϕ_e	0.4
Fraction of membrane in the cathode catalyst layer, l_m	0.4
Catalyst layer flooding (%)	100
Catalyst loading per unit area, m_{Pt} (mg/cm^2)	0.3
Fraction of catalyst, f_{Pt}	0.2
Membrane conductivity, σ_m (S/cm)	0.17
Density of platinum, ρ_{Pt} (g/cm^3)	21.5
Density of carbon black, ρ_c (g/cm^3)	2.0
Reference oxygen concentration, $C_{O_2,ref}$ (mol/m^3)	12
Transfer coefficient, α	0.5
Mixed electrode potential, E_{mixed} (V)	0.175

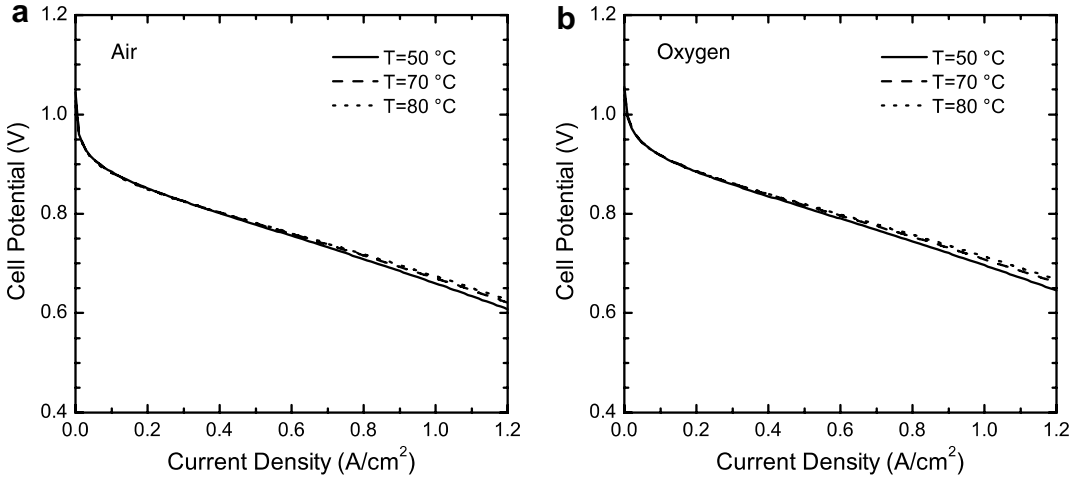

Fig. 9. Effect of temperature on the performance of PEM fuel cell for a flooded cathode catalyst layer at the base conditions operating at 3 atm with (a) air as the cathode gas, and (b) oxygen as the cathode gas.

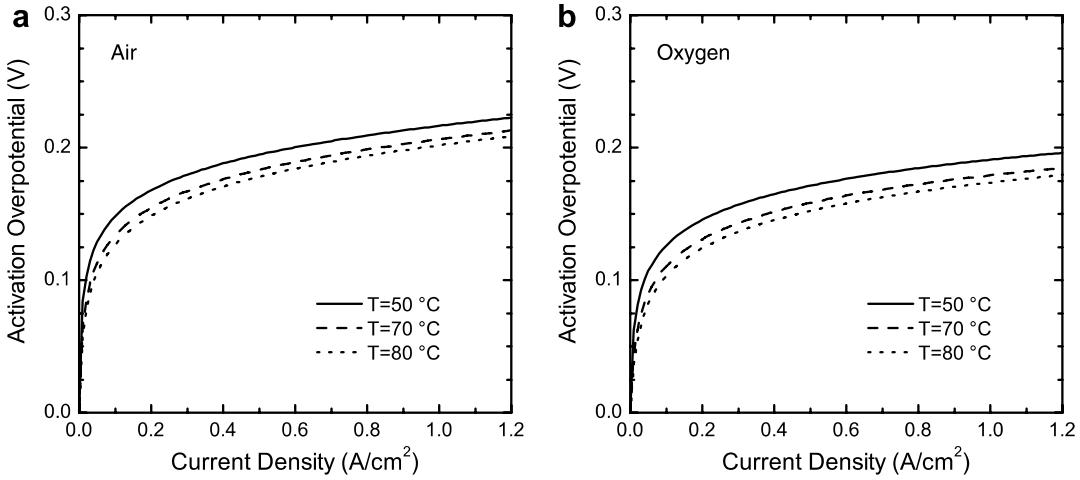

Fig. 10. Variation of the activation overpotential with current density at the base conditions for (a) air as the cathode gas, and (b) oxygen as the cathode gas for three different temperatures as indicated in the legend.

polarization with temperature. Fig. 10 shows the variation of the activation overpotential with current density for air as the cathode gas (Fig. 10a), and oxygen as the cathode gas (Fig. 10b) for three different temperatures as indicated in the legend. For both cases, similar trend has been observed in the activation overpotential as it increases with the temperature. Furthermore, Fig. 11 illustrates how the ohmic overpotential varies with the current density when temperature changes. Similar to the activation overpotential, ohmic overpotential also decreases with increasing temperature. Hence, temperature always reduces the total losses for PEM fuel cell, though cell performance did not improve accordingly due to the reduction of reversible cell potential. As seen from the present result, reversible cell potential decreases about 27 mV; and the activation and the ohmic overpotential decrease about 16 mV and 21 mV, respectively, at $J = 0.8$ A/cm^2 for an increase of temperature from 50 °C to 80 °C.

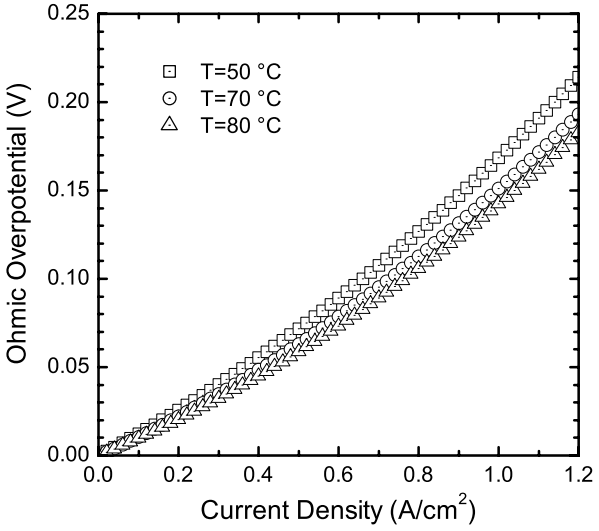

Fig. 11. Variation of the ohmic overpotential with current density at the base conditions for three different temperatures as indicated in the legend.

The effect of operating pressure on the cell potential for an un-flooded electrode and fully-flooded catalyst layer of PEM fuel cell is shown in Fig. 12. These results are modeled using the identical parameters as used in Fig. 9. It is seen that the cell potential increases with the cell operating pressure, and are consistent with the results reported in the literature [25]. As the empirical correlation of the ohmic overpotential is independent of cell operating pressure, these changes are purely due to the reduction in activation overpotential with pressure. However, in reality, pressure will affect the water flooding, and hence, the ohmic overpotential. The corresponding variations of activation overpotential with pressure are shown for air in Fig. 13a, and for oxygen in Fig. 13b. These results suggest that by increasing pressure from 1 atm to 5 atm, it is possible to attain almost 20% reduction in activation overpotential at $J = 0.8$ A/cm^2. The analytical expression derived for the activation overpotential does not have any pressure term, hence these reductions are mainly due to the change in oxygen concentration with pressure. Also higher pressure represents higher diffusion coefficient of oxygen through the electrode and enhances cell performance. It is also evident from these results for the effect of the operating conditions that both pressure and temperature have significant effect on the activation overpotential, whereas the ohmic overpotential is only affected by temperature. Therefore, to improve the cell performance or to reduce the cell polarization, it is always important to optimize the activation losses than the ohmic losses. In the following subsections, the optimization of cathode catalyst layer, particularly membrane content, Pt-loading and size of the cathode catalyst layer and their optimization for optimum cell performance will be considered.

3.2.2. Platinum loading and its optimization

As mentioned earlier, one of the barriers to the commercialization of PEM fuel cell is its cost. This is largely due to

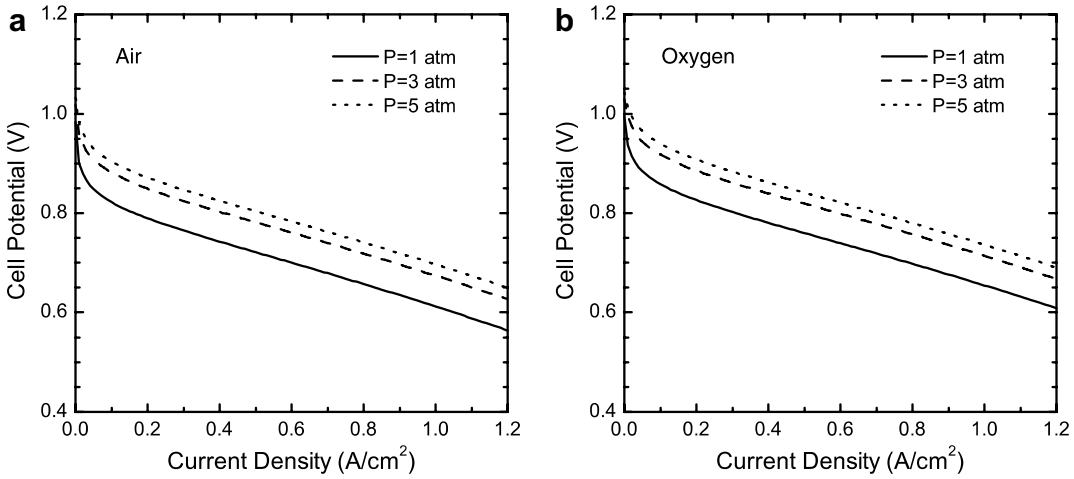

Fig. 12. Effect of pressure on cell performance for a fully-flooded cathode catalyst layer at the base conditions for (a) air as the cathode gas, and (b) oxygen as the cathode gas.

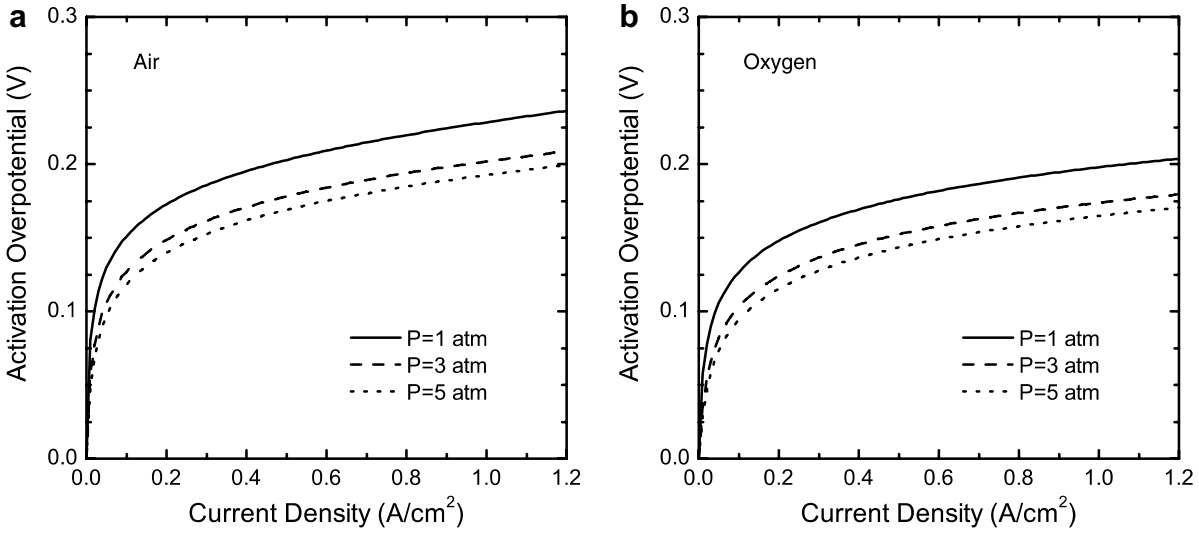

Fig. 13. Variation of the activation overpotential with current density at the base conditions for (a) air as the cathode gas, and (b) oxygen as the cathode gas for three different pressures as indicated in the legend.

the high Pt-loading, which is used as the catalyst in the cathode catalyst layer to promote the slow oxygen reduction reaction. Therefore, it is essential to reduce the amount of platinum in the catalyst layer while ensuring sufficient catalyst to enhance oxygen reduction reaction. In this section, the effect of Pt-loading on the cell potential as well as its optimization will be considered. Fig. 14 shows the variation of cell potential with current density with air as the oxidant in part (a), and oxygen as the oxidant in part (b), for five different Pt-loadings as indicated in the legend. The parameters used in this figure are listed in Table 5. The effect of Pt-loadings on the cell potential shows that an increase in the Pt-loading increases the cell potential for $m_{Pt} \leqslant 0.2$ mg/cm^2, while the cell potential drops with an increase in the Pt-loading for $m_{Pt} > 0.2$ mg/cm^2 for both air and oxygen. For instance, in Fig. 14a, the cell voltages are 0.7852, 0.7842, and 0.7817 V at 0.5 A/cm^2 for Pt-loadings of 0.2, 0.25, and 0.3 mg/cm^2, respectively. It is evident that increased amount of Pt-loading in the catalyst layer did not improve the oxygen reduction reaction or the cell performance for $m_{Pt} > 0.2$ mg/cm^2. This is largely due to the reduction in oxygen diffusion, due to the high Pt-content in the catalyst layer that blocks the passage for diffusion. In addition, excessive platinum does not always imply higher effective use of Pt-catalyst. It also reduces the reactive surface areas for oxygen reduction reaction that eventually reduces the cell performance at higher catalyst loadings.

Fig. 15 depicts the optimum Pt-loading as a function of the current density at a given cell potential of 0.8 V. Two parts of this figure represent the results of air as the cathode gas and oxygen as the cathode gas as mentioned in the figure. It is found that at the highest current density, the amount of Pt-loading is about 0.195 mg/cm^2 for both air

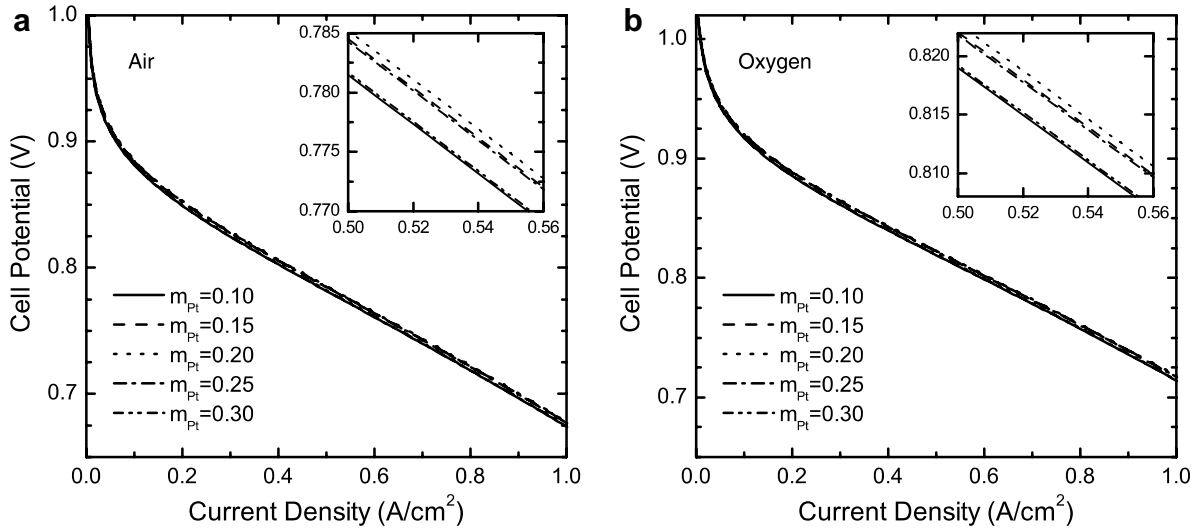

Fig. 14. Variation of the cell potential with current density at the base conditions for (a) air as the cathode gas, and (b) oxygen as the cathode gas for different platinum loadings as indicated in the legend.

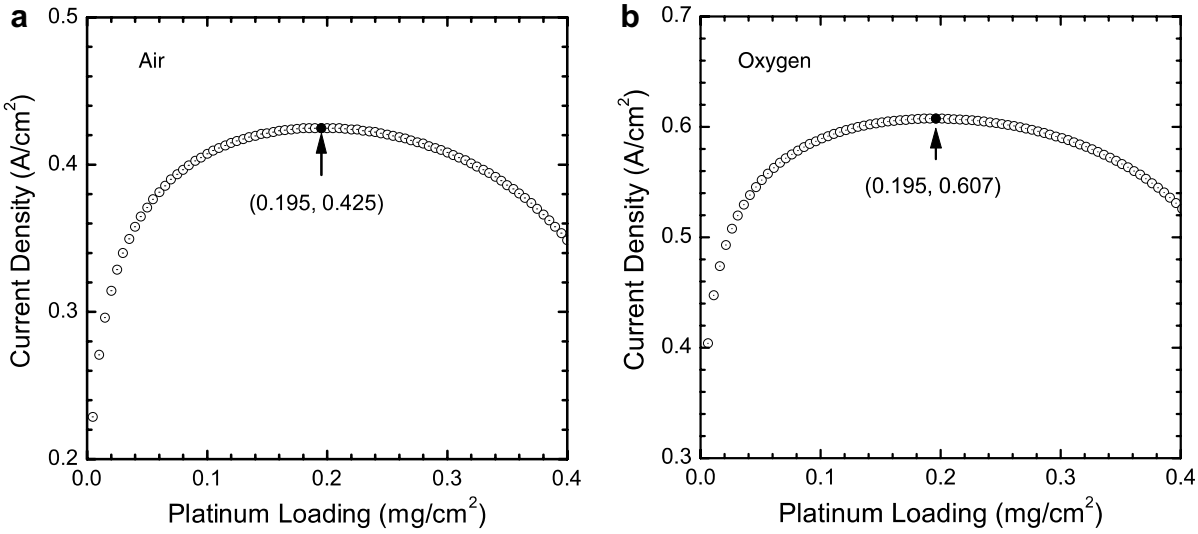

Fig. 15. Optimum platinum loading as a function of the current density at a given cell potential of 0.8 V for (a) air as the cathode gas, and (b) oxygen as the cathode gas.

and oxygen. It is close to the conclusion of Song et al. [34], though they found 0.21 mg/cm^2 of optimum Pt-loading for the given electrode potential of 0.6 V with completely different parameter values. It also reveals that for 0.4 mg/cm^2 Pt-loading, the cell power output decreases by about 20% for air and about 13% for oxygen compared to the optimum Pt-loading case. Clearly, optimization not only reduces the cost of the fuel cell but also improves the performance. Once again, Song et al. [34] obtained their results using complicated agglomerate model, which also requires numerical solution to a set of governing equations; whereas the present analytical model is easier for practical applications.

3.2.3. *Effect of membrane content in the catalyst layer*

The effect of the various amounts of membrane contents in the cathode catalyst layer is shown in Fig. 16 for air and oxygen as the cathode gas as indicated in the figure. In these figures, the amount of Pt-loading is used as 0.2 mg/cm^2 and all other parameters are the same as listed in Table 5. The results shown in these figures indicate that an increase in the membrane content in the catalyst layer increases the cell potential for both air and oxygen. This is due to the reduction in the resistance to proton transport to the reaction sites, consequently reducing the activation overpotential with higher membrane content in the catalyst layer. Here an empirical formulation is used for the ohmic overpotential that is a function of current and cell temperature only. Hence, changing the amount of membrane did not change the corresponding ohmic overpotential. Generally, higher membrane content reduces resistance to proton transport but would increase resistance to oxygen transport – a balance gives the "best" or "optimal" membrane content in the catalyst layer.

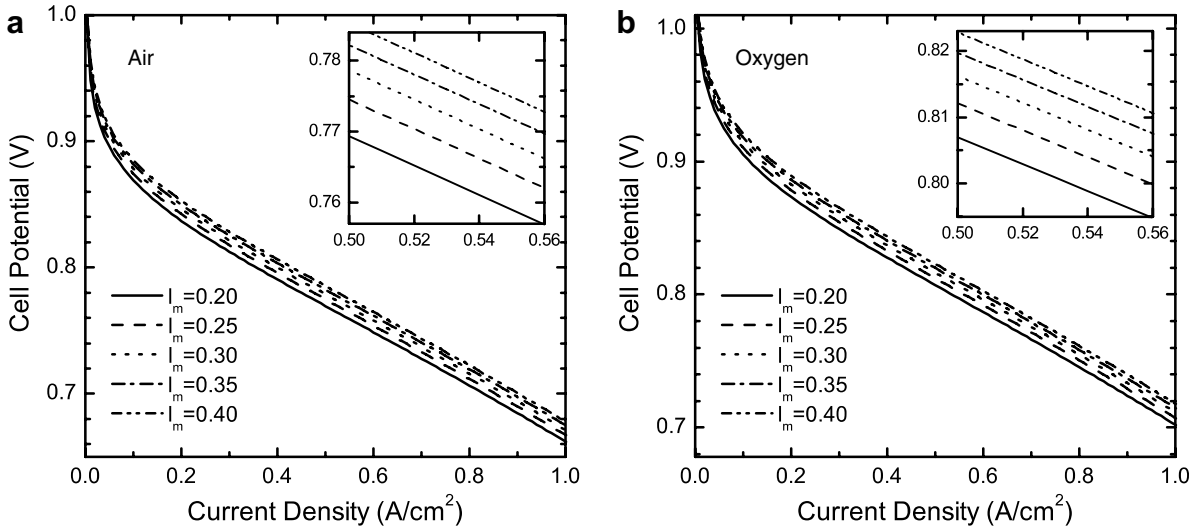

Fig. 16. Effect of membrane content in the catalyst layer on cell potential for (a) air as the cathode gas, and (b) oxygen as the cathode gas with a platinum loading of 0.2 mg/cm^2.

3.2.4. Optimization of catalyst layer thickness

Conflicting observations have been reported in the literature for the effect of catalyst layer thickness on the cell potential. It has been claimed that thicker catalyst layer can generate higher current [33] as well as the polarization of PEM fuel cell increases with the increase of the catalyst layer thickness because of the limited rate of mass diffusion [22]. It seems the second statement will be more appropriate as the mass diffusion rate is reduced with the catalyst layer thickness. In this section, the effect of catalyst layer thickness on the cell performance using the present analytical formulation will be investigated. Fig. 17 shows the effect of catalyst layer thickness on the cell output for air and oxygen as the cathode gas with a Pt-loading of 0.2 mg/cm^2. Five different catalyst layer thicknesses were considered as indicated in the legend. All other parameters are the same as listed in Table 5. For a given Pt-loading, it is shown that the cell potential increases rapidly with the increase of the catalyst layer thickness for $\delta_c \leqslant 10$ μm. For $\delta_c > 10$ μm, the results are completely opposite as the cell potential decreases slowly with the increase of the catalyst layer thickness due to the limited rate of mass diffusion in the catalyst layer as well as lower active surface area per unit volume. One might also question that the increase of catalyst layer thickness will also increase the ohmic overpotential and hence it is almost impossible to obtain better cell performance with thicker catalyst layer like Wang et al. [33] found. It is also noted that the ohmic overpotential formulation used in this study is independent of catalyst layer thickness. Therefore, the changes observed

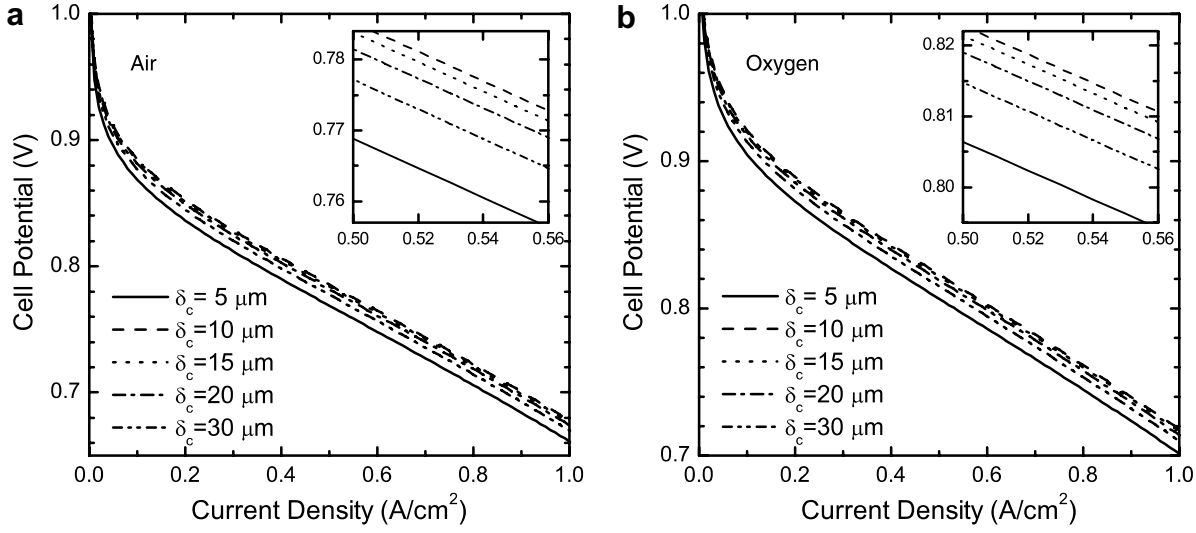

Fig. 17. Variation of the cell potential with current density for (a) air as the cathode gas, and (b) oxygen as the cathode gas with a platinum loading of 0.2 mg/cm^2 for different catalyst layer thicknesses as indicated in the legend.

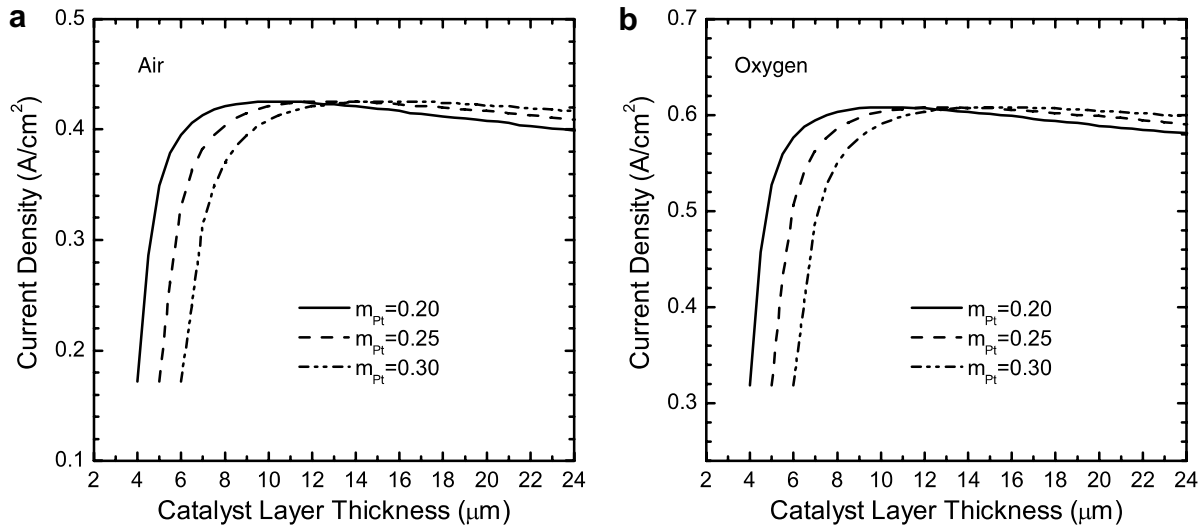

Fig. 18. Current density as a function of catalyst layer thickness at a given cell potential of 0.8 V for (a) air as the cathode gas, and (b) oxygen as the cathode gas for different platinum loadings as indicated in the legend.

in the cell potential is purely due to the change of activation overpotential. When the catalyst layer thickness is increased, it decreases the catalyst reactive surface area per unit volume since the Pt-loading per unit area is constant; and hence increases the activation overpotential.

To provide clearer evidence how the catalyst layer thickness affect the cell potential, the cell current density is plotted as a function of catalyst layer thickness. Fig. 18 shows the variation of current density with catalyst layer thickness for a given electrode potential of 0.8 V for air (Fig. 18a) and oxygen (Fig. 18b) as the cathode gas. Here three lines represent different Pt-loadings as indicated in the legend and all other parameters are identical to the conditions for Fig. 17. It is seen again that with the increase of the catalyst layer thickness, initially the cell current density increases rapidly and then decreases slowly after reaching a certain catalyst thickness for both the air and the oxygen cases. The thickness corresponding to highest current density is the optimum thickness of the catalyst layer for that Pt-loading. It is found that the optimum thicknesses are 10.5 ± 1, 13 ± 1.5, and 15.75 ± 1.75 μm for $m_{Pt} = 0.2$, 0.25, and 0.3 mg/cm^2, respectively. It also implies that the higher the Pt-loading the wider the optimum zone of the catalyst layer thickness and the higher the optimum catalyst layer thickness. Therefore, it is always desirable to design PEM fuel cells in the vicinity of optimum zone that will eventually decrease the cost with better cell performance.

4. Conclusions

An analytical formulation of the activation overpotential in the cathode catalyst layer of PEM fuel cells has been developed in this study. Water flooding in the catalyst and electrode backing layers is also taken into account, and comprehensive comparison has been made with empirical, experimental and numerical results. It has been shown that the present method is capable of predicting the fuel cell performance accurately. Then performance optimization of cathode catalyst layer in a PEM fuel cell has been carried out. It is found that catalyst layer performance is much more sensitive to the thickness of the catalyst layer than the other parameters, particularly below the optimum thickness. Reducing the size of the catalyst layer will reduce the cell cost without changing the cell performance. The model results also show that changing the catalyst layer thickness and the Pt-loading in the catalyst layer can provide an optimum value compared to the other operating and physical parameters. The optimum catalyst loading is found to be 0.195 mg/cm^2 for either air or oxygen as the cathode gas with a membrane content of 0.4% and 20% wt. Pt/C. The optimum catalyst layer thicknesses are found to be 10.5 ± 1, 13 ± 1.5, and 15.75 ± 1.75 μm for 0.2, 0.25, and 0.3 mg/cm^2 of Pt-loadings, respectively, with 40% membrane content and 20% wt. Pt/C in the catalyst layer.

Acknowledgements

This study is financially supported by the Natural Sciences and Engineering Research Council of Canada (NSERC). One of the authors (P.K.D.) also acknowledges a financial support from the NSERC as Canada Graduate Scholarship.

Appendix A. Calculation of diffusion coefficients

The binary diffusion coefficient of oxygen and nitrogen (cm^2/s) is calculated using Chapman–Enskog formula [39]

$$D_{O_2-H_2} = 0.00188 \frac{T^{3/2}\left(\frac{1}{M_{O_2}} + \frac{1}{M_{N_2}}\right)^{1/2}}{P\lambda^2_{O_2-N_2}\Omega_{D,O_2-N_2}} \quad (55)$$

Table 6
Parameter used in the calculations of diffusion coefficients at 3 atm and 80 °C

Variable	Value
Ω_{D,O_2-N_2}	0.8827
$\lambda_{O_2-N_2}$	3.6325
$T^{cr}_{O_2}$(K)	154.4
$P^{cr}_{O_2}$(atm)	49.7
$T^{cr}_{H_2O}$(K)	647.15
$P^{cr}_{H_2O}$(atm)	217.7
μ_{H_2O}(Pa s)	0.355×10^{-3}
V_{O_2}(cm^3/g mol)	25.6

where M_{O_2} and M_{N_2} are the molecular weights of oxygen and nitrogen, respectively. Ω_{D,O_2-N_2} is a dimensionless function of the temperature and of the intermolecular potential field of one molecule of O_2 and one of N_2, $\lambda_{O_2-N_2}$ is the Lennard–Jones parameter, and temperature T is in K. The binary diffusion coefficient of oxygen and water vapor in cm^2/s is calculated from the critical pressure and temperature of oxygen ($T^{cr}_{O_2}$ and $P^{cr}_{O_2}$) and water vapor ($T^{cr}_{H_2O}$ and $P^{cr}_{H_2O}$) using the Slattery–Bird equation [40]

$$PD_{O_2-H_2O} = 0.000364\left(\frac{T}{\sqrt{T^{cr}_{O_2}T^{cr}_{H_2O}}}\right)^{2.334} \times \left(P^{cr}_{O_2}P^{cr}_{H_2O}\right)^{1/3}\left(T^{cr}_{O_2}T^{cr}_{H_2O}\right)^{5/12}\left(\frac{1}{M_{O_2}}+\frac{1}{M_{H_2O}}\right)^{1/2} \quad (56)$$

where the temperatures are in Kelvin and the pressures are in atm.

The binary diffusion coefficient in cm^2/s for oxygen in liquid water ($H_2O_{(l)}$) is obtained using Wilke–Chang equation [39]

$$D_{O_2-H_2O_{(l)}} = \frac{7.4\times10^{-11}(\Phi M_{H_2O})^{1/2}T}{\mu_{H_2O}(V_{O_2})^{0.6}} \quad (57)$$

where μ_{H_2O} is the dynamic viscosity of H_2O in Pa s, Φ is the "association" parameter of H_2O, V_{O_2} is the molar volume of the O_2 in cm^3/g mol at its normal boiling point. The value of Φ for water was originally reported as 2.6, later it was found using the empirical best fit as 2.26. Therefore, in the present investigation 2.26 is used instead of 2.6.

The diffusion coefficient (cm^2/s) for oxygen in Nafion® membrane is calculated from the following relation [22]

$$D_{O_2-m} = -1.0664\times10^{-5} + 9.0215\times10^{-6} \times \exp\left(\frac{T-273.15}{106.65}\right) \quad (58)$$

where the temperature T is in Kelvin. Values for parameters used in the above equations are listed in Table 6 with appropriate units.

References

[1] P. Costamagna, S. Srinivasan, J. Power Sources 102 (2001) 242.
[2] P. Costamagna, S. Srinivasan, J. Power Sources 102 (2001) 253.
[3] X. Li, Principles of Fuel Cells, Taylor & Francis, New York, 2006.
[4] D.M. Bernardi, M.W. Verbrugge, AIChE J. 37 (1991) 1151.
[5] D.M. Bernardi, M.W. Verbrugge, J. Electrochem. Soc. 139 (1992) 2477.
[6] N.P. Siegel, M.W. Ellis, D.J. Nelson, M.R. von Spakovsky, J. Power Sources 115 (2003) 81.
[7] J.J. Baschuk, X. Li, J. Power Sources 86 (2000) 181.
[8] M.W. Verbrugge, R.F. Hill, J. Electrochem. Soc. 137 (1990) 886.
[9] T.E. Springer, T.A. Zawodzinski, S. Gottesfeld, J. Electrochem. Soc. 138 (1991) 2334.
[10] T.E. Springer, M.S. Wilson, S. Gottesfeld, J. Electrochem. Soc. 140 (1993) 3513.
[11] V. Gurau, H.T. Liu, S. Kakac, AIChE J. 44 (1998) 2410.
[12] M. Eikerling, Y.I. Kharkats, A.A. Kornyshev, Y.M. Volfkovich, J. Electrochem. Soc. 145 (1998) 2684.
[13] T. Thampan, S. Malhotra, H. Tang, R. Datta, J. Electrochem. Soc. 147 (2000) 3242.
[14] S. Um, C.Y. Wang, K.S. Chen, J. Electrochem. Soc. 147 (2000) 4485.
[15] N.P. Siegel, M.W. Ellis, D.J. Nelson, M.R. von Spakovsky, J. Power Sources 128 (2004) 173.
[16] G. Karimi, X. Li, J. Power Sources 140 (2005) 1.
[17] S. Um, C.Y. Wang, J. Power Sources 125 (2004) 40.
[18] G.J.M. Janssen, J. Electrochem. Soc. 148 (2001) A1313.
[19] M.R. Hu, A.Z. Gu, M.H. Wang, X.J. Zhu, L.J. Yu, Energy Convers. Manage. 45 (2004) 1861.
[20] L.X. You, H.T. Liu, J. Power Sources 155 (2006) 219.
[21] Y. Wang, C.Y. Wang, J. Electrochem. Soc. 153 (2006) A1193.
[22] C. Marr, X. Li, J. Power Sources 77 (1999) 17.
[23] R. Sousa, E.R. Gonzalez, J. Power Sources 147 (2005) 32.
[24] A.F. Gulla, M.S. Saha, R.J. Allen, S. Mukerjee, J. Electrochem. Soc. 153 (2006) A366.
[25] C. Marr, X. Li, ARI 50 (1998) 190.
[26] J. Kim, S.M. Lee, S. Srinivasan, C.E. Chamberlin, J. Electrochem. Soc. 142 (1995) 2670.
[27] A. Rowe, X. Li, J. Power Sources 102 (2001) 82.
[28] J.C. Amphlett, R.M. Baumert, R.F. Mann, B.A. Peppley, P.R. Roberge, T.J. Harris, J. Electrochem. Soc. 142 (1995) 1.
[29] J.C. Amphlett, R.M. Baumert, R.F. Mann, B.A. Peppley, P.R. Roberge, T.J. Harris, J. Electrochem. Soc. 142 (1995) 9.
[30] G. Squadrito, G. Maggio, E. Passalacqua, F. Lufrano, A. Patti, J. Appl. Electrochem. 29 (1999) 1449.
[31] M. Eikerling, A.A. Kornyshev, J. Electroanal. Chem. 453 (1998) 89.
[32] Z.N. Farhat, J. Power Sources 138 (2004) 68.
[33] Q.P. Wang, D.T. Song, T. Navessin, S. Holdcroft, Z.S. Liu, Electrochim. Acta 50 (2004) 725.
[34] D.T. Song, Q.P. Wang, Z.S. Liu, T. Navessin, M. Eikerling, S. Holdcroft, J. Power Sources 126 (2004) 104.
[35] K.M. Yin, J. Electrochem. Soc. 152 (2005) A583.
[36] M. Eikerling, A.A. Kornyshev, A.M. Kuznetsov, J. Ulstrup, S. Walbran, J. Phys. Chem. B 105 (2001) 3646.
[37] A. Parthasarathy, S. Srinivasan, A.J. Appleby, C.R. Martin, J. Electrochem. Soc. 139 (1992) 2530.
[38] E-TEK. Gas Diffusion Electrodes and Catalyst Materials Catalogue, 1995.
[39] R.H. Perry, D.W. Green, Perry's Chemical Engineers' Handbook, McGraw-Hill, New York, 1997.
[40] R.B. Bird, W.E. Stewart, E.N. Lightfoot, Transport Phenomena, Wiley, New York, 1960.
[41] C. Stone, in: Proceedings of International Green Energy Conference, Waterloo, Ont., Canada, 2005.